Advancing Preclinical Biology for Ewing Sarcoma: An International Effort

Filemon S. Dela Cruz[1], Elizabeth A. Stewart[2,3], Didier Surdez[4], Jessica D. Daley[5], Alice Soragni[6], Eleni M. Tomazou[7,8], Jaime Alvarez-Perez[1], Tamar Y. Feinberg[1], James F. Amatruda[9,10], Shireen S. Ganapathi[11,12], Joyce E. Ohm[13], Christine M. Heske[14], Sarah Cohen-Gogo[15,16], Dusan Pesic[16], Joshua O. Nash[16], Adam Shlien[16], Elizabeth A. Roundhill[17], Susan A. Burchill[17], Brian D. Crompton[18], Elizabeth R. Lawlor[11,12], David M. Loeb[19,20], Olivier Delattre[21], Jaume Mora[22], Katia Scotlandi[23], Damon R. Reed[1], Patrick J. Grohar[24], Thomas G.P. Grünewald[25,26,27,28], Heinrich Kovar[7,29], and Kelly M. Bailey[5]

ABSTRACT

Ewing sarcoma is an aggressive bone and soft-tissue cancer affecting adolescents and young adults. *In vitro* and *in vivo* models of Ewing sarcoma have been instrumental in advancing our understanding of Ewing sarcoma biology and essential in evaluating potential therapies, particularly for metastatic or relapsed disease for which effective treatment options remain limited. Through an international collaborative effort between the Children's Oncology Group Bone Tumor Committee and the Euro Ewing Consortium, we review the current landscape of preclinical modeling used in Ewing sarcoma research encompassing both *in vitro* (cell lines and tumor organoids) and *in vivo* (mouse and nonmammalian xenografts) model systems. We discuss factors that can influence experimental results, provide testing considerations for both *in vitro* and *in vivo* studies, and descriptions of existing preclinical data repositories. We highlight current needs in Ewing sarcoma modeling and the importance of enhanced international cooperative research and patient advocacy efforts which will be critical in expanding our resources of biologically relevant Ewing sarcoma models to enable translation of preclinical findings into effective therapeutic strategies for patients with Ewing sarcoma.

Introduction

Treatments to improve survival for metastatic and relapsed Ewing sarcoma, a bone and soft-tissue sarcoma of adolescents and young adults, remain elusive despite large, international efforts. Thanks to continued work to conduct both somatic and germline sequencing and retrospective studies associating certain molecular alterations with clinical outcomes, prognostic molecular features in Ewing sarcoma are emerging and advancing our understanding of Ewing sarcoma heterogeneity. Recurrent molecular alterations, including, but not limited to, *STAG2* loss, *TP53*-inactivating mutations, and copy-number variations (CNV), contribute to the biological heterogeneity of Ewing sarcoma (1). Advances in our understanding of Ewing sarcoma biology coupled with the development of improved model systems to identify and validate potential therapeutics provide a renewed opportunity for discovery. Acknowledging the value of understanding the breadth of

[1]Department of Pediatrics, Memorial Sloan Kettering Cancer Center, New York, New York. [2]Department of Oncology, St. Jude Children's Research Hospital, Memphis, Tennessee. [3]Department of Developmental Neurobiology, St. Jude Children's Research Hospital, Memphis, Tennessee. [4]Balgrist University Hospital, Faculty of Medicine, University of Zurich (UZH), Zurich, Switzerland. [5]University of Pittsburgh School of Medicine, Pittsburgh, Pennsylvania. [6]Department of Orthopaedic Surgery, David Geffen School of Medicine, University of California Los Angeles, Los Angeles, California. [7]St. Anna Children's Cancer Research Institute, Vienna, Austria. [8]Medical University of Vienna, Center for Cancer Research, Vienna, Austria. [9]Cancer and Blood Disease Institute, Children's Hospital Los Angeles, Los Angeles, California. [10]Department of Pediatrics, Keck School of Medicine, University of Southern California, Los Angeles, California. [11]Ben Towne Center for Childhood Cancer and Blood Disorders Research, Seattle Children's Research Institute, Seattle, Washington. [12]Department of Pediatrics, Seattle Children's Hospital, Fred Hutch Cancer Center, University of Washington, Seattle, Washington. [13]Department of Cancer Genetics and Genomics, Roswell Park Comprehensive Cancer Center, Buffalo, New York. [14]Pediatric Oncology Branch, Center for Cancer Research, National Cancer Institute, Bethesda, Maryland. [15]Division of Hematology/Oncology, Department of Pediatrics, The Hospital for Sick Children, Toronto, Canada. [16]Genetics and Genome Biology Program, The Hospital for Sick Children, Toronto, Canada. [17]Children's Cancer Research Group, Leeds Institute of Medical Research, University of Leeds, Leeds, United Kingdom. [18]Dana-Farber/Boston Children's Cancer and Blood Disorders Center, Boston, Massachusetts. [19]Department of Pediatrics, Cancer Dormancy Institute, Albert Einstein College of Medicine, Bronx, New York. [20]Department of Developmental and Molecular Biology, Cancer Dormancy Institute, Albert Einstein College of Medicine, Bronx, New York. [21]INSERM U830, Diversity and Plasticity of Childhood Tumors Lab, PSL Research University, SIREDO Oncology Center, Institut Curie Research Center, Paris, France. [22]Pediatric Cancer Center Barcelona (PCCB), Hospital Sant Joan de Déu, Barcelona, Spain. [23]Experimental Oncology Laboratory, IRCCS Istituto Ortopedico Rizzoli, Bologna, Italy. [24]Division of Hematology/Oncology, Department of Pediatrics, University of Michigan Medical School, Rogel Cancer Center, Ann Arbor, Michigan. [25]Division of Translational Pediatric Sarcoma Research, German Cancer Research Center (DKFZ), German Cancer Consortium (DKTK), Heidelberg, Germany. [26]Hopp Children's Cancer Center (KiTZ), Heidelberg, Germany. [27]National Center for Tumor Diseases (NCT), NCT Heidelberg, a partnership between DKFZ and Heidelberg University Hospital, Heidelberg, Germany. [28]Institute of Pathology, Heidelberg University Hospital, Heidelberg, Germany. [29]Department of Pediatrics, Medical University of Vienna, Vienna, Austria.

Corresponding Author: Kelly M. Bailey, University of Pittsburgh School of Medicine, 51122 Rangos Research Building, 4401 Penn Ave, Pittsburgh, PA 15224. E-mail: kelly.bailey@chp.edu

Mol Cancer Ther 2026;25:48–70

doi: 10.1158/1535-7163.MCT-25-0428

preclinical models for Ewing sarcoma, members of the Children's Oncology Group (COG) Bone Tumor Committee and the Euro Ewing Consortium (EEC) with expertise in Ewing sarcoma modeling and biology engaged in a collaborative effort to collate a comprehensive, annotated collection of currently available Ewing sarcoma *in vitro*, *ex vivo*, and *in vivo* preclinical models. In addition, shared Ewing sarcoma data repositories are detailed. Perspectives on the benefits of specific models are presented, and the need to improve representation of diverse patient-derived Ewing sarcoma cells and tissues in preclinical therapeutic studies is discussed. This international effort is intended to serve as a resource to advance thoughtful planning of future preclinical studies and encourage continued data sharing across the community.

In vitro Modeling of Ewing Sarcoma

To date, the development of a genetically engineered mouse model (GEMM) of Ewing sarcoma has been unsuccessful and engraftment of human Ewing sarcoma cells in mice is inefficient (24%–50% engraftment; refs. 2–4). Coupled with a moral obligation to reduce the use of animals in research and an international desire to minimize the costs of preclinical drug testing, several groups have developed multicellular *in vitro* models with the goal of generating preclinical tools to increase the efficiency of therapeutic discovery and prioritization of drugs for evaluation in clinical trials (5, 6). These *in vitro* models range from simple two-dimensional (2D) cell lines to more complex three-dimensional (3D) models and use both well-characterized Ewing sarcoma cell lines that have been in culture for >40 years and low-passage cell lines more recently derived from patients with Ewing sarcoma. We hypothesize that these newer models will provide more physiologically relevant tools to evaluate small-molecule and cellular therapies and improve the efficiency of identifying promising therapies for evaluation in clinical trials.

2D cell line models of Ewing sarcoma

Over the past several decades, academic institutions, translational research centers, and commercial entities have spearheaded the expansion, production, and availability of numerous patient-derived Ewing sarcoma cell lines for preclinical investigations. In contrast to the extensive heterogeneity and varied molecular landscape of other carcinoma and sarcoma cell lines, Ewing sarcoma tumor genomes are less complex, have a low mutational burden, and are defined by reciprocal translocations between the *EWSR1* gene on chromosome (chr) 22 and the *FLI1* gene on chr 11 or other members of the ETS family of transcription factors, including *ERG*, *ETV1*, and *FEV* (7, 8). The resulting gene fusions operate as chimeric oncogenic transcription factors to rewire the transcriptome and epigenome of Ewing sarcoma tumor cells, both inducing and repressing transcription (9). Elegant work has described that the amount or level of EWS::FLI1 can dynamically change in Ewing tumor cells, resulting in behaviorally distinct cell states such as migratory EWS::FLI1 "low" and proliferative EWS::FLI1 "high" states (10). In addition, excess EWS::FLI1 expression is overtly toxic to cells (11, 12). The shifts in cellular function related to the EWS::FLI1 expression level lend to difficulties in both disease modeling and therapeutically targeting the fusion oncoprotein (2, 13).

Broad cataloging of deposited, published, or commercially available Ewing sarcoma cell lines reveals the generation of 47 cell lines harboring *EWSR1::FLI1* fusions, with 20 between *EWSR1* exon 7 and *FLI* exon 6, 11 between *EWSR1* exon 7 and *FLI1* exon 5, and eight cell lines harboring *EWSR1::ERG* fusions (**Table 1**). Consistent with prior work, compilation of the associated genomic and transcriptomic sequencing data shows the most frequent mutations detected in cell lines are in the cohesin complex subunit *STAG2*, *CDKN2A*, and *TP53*—molecular alterations often coincident with poor patient outcomes (**Table 1**; refs. 7, 8).

Importantly, short tandem repeat (STR) DNA profiling of established Ewing sarcoma cell lines has grown in importance as an effort across research groups to annotate, authenticate, and validate cultured cell lines for preclinical studies. Of note, multiple patient-derived Ewing sarcoma cell lines have differing STR profiles depending on the institutional and commercial resource. This divergence is evident in 11 of 52 cell lines with available STR profiles (A-673, CADO-ES1, CHLA-32, CHLA-258, CHLA-352, CHP100, EW-8, MHH-ES-1, SK-ES-1, SK-N-MC, and TC71) with discrepancies in distinct STRs listed in the Cellosaurus database (Supplementary Table S1). Although five of the 11 cell lines (A-673, CHP100, CHLA-258, MHH-ES-1, and SK-ES-1) only show variations in one STR, three of the 11 cell lines (CHLA-352, SK-N-MC, and TC-71) show variations in multiple STRs (Supplementary Table S1). These discrepancies in STR allele copy numbers and frequencies for well-characterized cell lines indicate genetic drift, differences in passage number, clonal selection, and institution-dependent determinations of CNVs and loss of heterozygosity. Despite these data and the ongoing challenges in cataloging information about cell line passage number, recent evidence supports the relative genomic and transcriptomic stability of many established Ewing sarcoma cell lines over time (14). Furthermore, multiomics efforts across Ewing sarcoma cell lines to characterize Ewing sarcoma fusion–driven gene regulation show preserved core transcriptional signatures that are both induced and repressed in an Ewing sarcoma fusion–dependent manner (9).

Interestingly, there is ample evidence that carcinoma cell lines derived from genetically complex cancers such as cervical and breast cancers may undergo substantial genetic evolution in long-term culture, thus compromising reproducibility of experimental results. Conversely, at least some Ewing sarcoma cell lines seem to be genetically, transcriptionally, and phenotypically stable in culture (14). Indeed, even though there is a spectrum of stability among Ewing sarcoma cell lines, even one of the most widely used cell lines A-673 that harbors a *BRAF* mutation (V600E)—an atypical event in Ewing sarcoma—in addition to the driver oncogene *EWSR1::FLI1* seemed to be much more stable than carcinoma cell lines (14).

3D spheroid models of Ewing sarcoma

Spheroids are simple, self-organizing aggregates of tumor cells—typically formed without added extracellular matrix (ECM) and cultured in low-attachment conditions using Ewing sarcoma cell lines or low-passage primary cells. Spheroid cultures recapitulate several features of tumors, including the hypoxic tumor microenvironment (TME; the surrounding nonmalignant cells and matrix that influence tumor growth, progression, and treatment response) and 3D cell–cell interactions, which are absent in 2D cultures (15, 16). These are matrix-free models typically grown in low-attachment plates and established from either established commercially available cell lines or from passaged or unpassaged primary patient-derived cells. Over the past two decades, several studies have demonstrated the use of 3D spheroids from Ewing sarcoma cell lines (16–18). Recently, a practical approach to culture Ewing sarcoma cell line models in 3D spheroid cultures in media that better mimic the metabolite composition of human plasma (i.e., physiologic media) has been described, which more faithfully

recapitulates the characteristics of patient tumors (16). Hence, despite the limitations of cancer cell lines in general, Ewing sarcoma cell lines, if grown under appropriate conditions (3D and in physiologic media), are readily propagatable and serve as genetically stable models that continue to be the workhorse of Ewing sarcoma research.

Ewing sarcoma spheroid models generated from primary patient-derived Ewing sarcoma tissue (PDES) can be readily established and, in some cases, propagated on plastic. In contrast to established cell lines, PDES do not have limitless replicative capacity. Moreover, the transcriptome of these cells clusters independently from established cell lines (19). Consistent with the importance of the ECM in Ewing sarcoma biology (20), PDES express and secrete proteins associated with organization of the ECM, including fibrillin-1, collagen type VI alpha 3 chain, integrin subunit beta 1, collagen type VI alpha 2 chain, and collagen type VI alpha 1 chain (21). PDES form multicellular 3D structures when seeded in low-adherence conditions (19). PDES 3D structures may be useful tools to investigate the efficacy of candidate new treatment combinations and increase understanding of how best to combine treatments for patient benefit. In contrast to rapidly proliferating established cell lines which are sensitive to chemotherapeutic agents targeting dividing cells, PDES models are more resistant (19). The effect of drugs on PDES seems to more closely reflect the clinical response and outcomes of patients from whom they were derived than those reported in established cell lines.

However, spheroids do not fully model the complexity of the Ewing sarcoma microenvironment, which affects response and systemic drug delivery in patients (22–24). To overcome this limitation, some groups are combining spheroids with scaffolds to mimic the bone microenvironment or developing matrix-embedded tumoroid models (25). These models have the advantage of combining tumor cells with cells of the TME under physiologic mechanical stresses, which can affect tumor growth, metastasis, and drug delivery (25).

Patient-derived tumor organoid models of Ewing sarcoma

In contrast to spheroid models, tumor organoids are multicellular models that recapitulate cellular heterogeneity (incorporating tumor cells and cells of the TME), spatial organization, and the molecular and functional features of the tissues from which they are derived (26). Patient-derived tumor organoids (PDTO), also referred to as tumoroids, can be established directly from cancer cells obtained from surgical biopsies or resections (26–28). A key advantage of these models is their ability to incorporate the ECM and preserve cell–cell interactions, while also mimicking patient-specific therapy responses (26, 27, 29–32). The suitability of PDTOs for drug response screening has driven its use in drug development and precision medicine (26, 33). PDTOs offer a platform for cost-effective, high-throughput, rapid drug screening (Research Square rs.3.rs-5039845/v1; ref. 34). To enable a more accurate representation of tumor complexity for translational research, PDTOs can be cultured short term to preserve the heterogeneous cell populations of the original tumor, which are lost during extended culture and passaging (Research Square rs.3.rs-5039845/v1; refs. 28, 34). In contrast, long-term passaged PDTOs serve as expandable and shareable resources that can facilitate in-depth investigations into tumor biology (Research Square rs.3.rs-5039845/v1; ref. 34).

Although PDTOs have been developed for most epithelial cancers, progress in establishing sarcoma organoid models has only recently gained momentum. A recent article described the establishment of more than 100 patient-derived sarcoma organoid models across more than 20 histologies, including Ewing sarcoma, leveraging a specific geometry compatible with high-throughput rapid drug screening (34). These unpassaged models maintain the cellular diversity of the TME, preserve key molecular features, and recapitulate patient-specific responses (34, 35).

Short-term PDTO models offer several advantages, such as preserving microenvironmental cell components beyond tumor cells and minimizing clonal selection and *de novo* loss or acquisition of mutations and CNVs, which can increase with extended culture (34, 36–38). Moreover, short-term PDTOs can be generated from indolent, slow-growing sarcomas, as well as pretreated cases (34, 36). This enables the possibility of modeling Ewing sarcomas that lack more aggressive features (e.g., *TP53* mutations), which are less likely to establish as patient-derived xenografts (PDX), as well as to develop a longitudinal series across the treatment history of a patient (34). Yet, short-term PDTOs are typically severely limited by the number of cells obtained from clinical samples. Therefore, it remains critically important to develop renewable models that can be maintained long term. Although short-term PDTOs lose cellular heterogeneity and become more akin to cell lines over time in culture, they offer the benefit of serving as a resource of tumor cells that can be propagated and shared with the research community to facilitate the study of Ewing sarcoma biology and drug responses in a more physiologically relevant system than traditional cell lines (Research Square rs.3.rs-5039845/v1). Feasibility to establish long-term Ewing sarcoma tumoroids was recently demonstrated (31). Both short- and long-term Ewing sarcoma PDTOs may also serve as a foundation for developing immunocompetent tumoroids by incorporating a patient's own immune cells, such as peripheral blood mononuclear cells, T cells, or tumor-infiltrating lymphocytes (39). These models could be utilized to investigate patient-specific responses to checkpoint inhibitors (39, 40). Additionally, chimeric antigen receptor T cells (CAR-T) can be introduced to evaluate responses either preclinically, during CAR-T development, and indication-finding studies, as well as for personalized approaches using approved CAR-T products (41).

Although efforts to establish sarcoma PDTOs have been limited to date, published protocols and the high success rates observed—particularly for short-term models—should encourage greater community-wide efforts in this field. The single most critical factor for advancing patient-derived models is access to tissue. Coordinated efforts through large collaborative organizations such as the COG and EEC, inclusion of procurement of research samples in ongoing trials, and collaborations with clinicians within and across research centers will be essential to overcome this barrier and further propel research in Ewing sarcoma tumoroid development.

Developing Ewing sarcoma models using human stem cells

Recent advancements in human pluripotent stem cell (hPSC) technologies and hPSC-based tumor modeling have enabled new insights into the oncogenic function of the EWS::FLI1 fusion protein (42–44). We now benefit from a wide array of hPSC lines and more efficient protocols for generating induced pluripotent stem cells (45), alongside advanced differentiation techniques that allow for the creation of hPSC-derived cells and organoids (46, 47), which can simulate various stages of human development. Moreover, combining these hPSC culture protocols with recent advancements in genome editing tools enables the systematic exploration of how cellular context and oncogenes interact in a high-throughput, unbiased manner (48). This is particularly relevant for pediatric

tumors, especially fusion-driven sarcomas like Ewing sarcoma (49, 50). Unlike other cancers that develop through stepwise accumulation of multiple genetic mutations, Ewing sarcoma arises from a single *EWSR1::ETS* chromosomal rearrangement, most frequently the *EWSR1::FLI1* fusion oncogene. This fusion protein is highly cancer specific and is deeply influenced by the epigenetic/genetic context provided by the cell of origin and its differentiation state. It is now clear that *EWSR1::FLI1* cannot indiscriminately transform all cells; rather, the unique combination of the cell of origin and the fusion protein dictates the cellular and clinical characteristics of the resulting Ewing sarcoma tumor (51–55).

Although hPSC-based protocols are still being refined, multilineage approaches offer a valuable expansion to the toolkit available for Ewing sarcoma research. It is now possible to generate multiple candidate Ewing sarcoma cells of origin through reprogramming, creating cell resources enabling the study of fundamental mechanisms of Ewing sarcoma biology both *in vitro* and *in vivo* (56). This approach holds the potential to develop powerful new models of the disease, providing unprecedented insights into the early stages of tumor formation—insights that are difficult to capture using existing patient-derived models.

Human mesenchymal stem cells (hMSC) are multipotent precursors that can be differentiated *in vitro* into various cell types, typically osteoblasts, chondrocytes, and adipocytes, but also along the endothelial linage. EWS::FLI1 overexpression in adult hMSCs blocks their differentiation and generates a transcriptome profile reminiscent of Ewing sarcoma (57). Many of these EWS::FLI1-regulated genes are more strongly induced when the oncogene is expressed in pediatric hMSCs (hpMSC), whereas numerous genes that are among the most prominent Ewing sarcoma markers are induced in hpMSCs but not in their adult counterparts (58). Notably, although hpMSCs provide a far more permissive environment, hpMSCs that express EWS::FLI1 are, like EWS::FLI1-expressing adult hMSCs, unable to form tumors *in vivo*. In addition to the age of the MSC donor, the anatomic site of MSC origin may affect susceptibility to EWS::FLI1-induced transformation as has been demonstrated for mouse osteochondrogenic precursors, which were found to be more susceptible when derived from the stylopod than from the zeugopod (59). Similarly, CRISPR-mediated *EWSR1::FLI1* translocation in MSCs is insufficient to generate transforming models within 1 year (60). However, the addition of *STAG2*, *TP53*, and *CDKN2A* mutations to this approach resulted in fully transforming models. Gordon and colleagues developed an approach that exploits the *in vitro* potential of hPSCs to differentiate into cells from the three germ layers when forming embryoid bodies (EB; ref. 36). EWS::FLI1 expression in EBs derived from p53-deficient human embryonic stem cells leads to *in vitro* transformation, yet EB-derived cells lack tumor formation capacities *in vivo* (36).

Challenges of *in vitro* models

Despite the tremendous advances in preclinical modeling of Ewing sarcoma in recent years, numerous challenges remain. First, because of standard treatment protocols and availability of clinical specimens, the field largely lacks paired models of diagnosis and relapse. Resolving this challenge will require concerted efforts to collect research-specific biopsies from patients beyond standard clinical protocols, an effort that will require community support from patients and their families to undergo additional procedures. The number of patient samples required to model the heterogeneity of Ewing sarcoma is yet to be determined and underscores the need for cooperative international efforts. Both serial models from the same patient to evaluate heterogeneity and resistance, in addition to more focused studies on residual populations, are expected to more clearly identify targets for therapy in resistance and minimal residual disease states.

In vivo Modeling of Ewing Sarcoma

GEMMs of Ewing sarcoma

GEMMs can recapitulate and model cancer initiation and evolution in an immune-competent background, providing dynamic insights into disease pathogenesis and tumor host interactions, ideally allowing for rapid preclinical drug testing. However, attempts to genetically model Ewing sarcoma in the mouse have been frustrating. Strategies introducing human EWS::FLI1 in limb bud mesenchyme, osteoblast precursors, neuronal tissue, or muscle, using a variety of promoters to drive the gene fusion and Cre lines to conditionally activate the transgene, resulted in either no phenotype at all, embryonic lethality, tissue damage, and/or developmental defects but not tumorigenesis (2, 61). These negative findings raised questions about context- and developmental stage–specific oncogene dosing and toxicity. As *de novo* gene activation via binding to GGAA microsatellites is a key pathogenic activity of EWS::FLI1, distinct GGAA microsatellite landscapes in mice and humans may explain the failure to generate Ewing sarcoma in mice. However, recent results obtained in *Drosophila*, zebrafish, and an early study driving EWS::FLI1 expression from the ubiquitous *ROSA26* locus with MxCre-mediated activation in adult mice suggest species-independent transforming activity of the fusion protein (62, 63). Torchia and colleagues induced EWS::FLI1 activation at post-natal days 2 to 3, whereas the majority of tested conditional EWS::FLI1 mouse models activated the fusion gene during embryogenesis with no resulting tumor formation (2). However, when targeted to the mesenchymal lineage of embryonal endochondral bone formation and activated in a narrow time window after birth, EWS::FLI1 expression resulted in Ewing sarcoma–like tumorigenesis with long latency (12, 64). Similarly, Tanaka and colleagues (65) demonstrated that mouse osteochondrogenic progenitors derived from the embryonic superficial zone of long bones collected from late gestational embryos and *ex vivo* transduced with EWS::FLI1 were able to form Ewing sarcoma–like tumors in nude mice. A recent study using embryonic mouse mesenchymal stem–like cells reports a two-step epigenetic mechanism of EWS::FLI1-driven tumorigenic transformation with the fusion oncogene causing immortalization and developmental arrest, followed by post-natal humoral tumor promotion identifying pubertal growth factors (i.e., high levels of insulin-like growth factor 1 and insulin) as candidate drivers of tumorigenesis (66). These results suggest that transplantation models of genetically engineered mice with EWS::FLI1 targeted to embryonal mesenchymal precursors may hold promise as alternative disease models for preclinical drug development.

Humanized mouse models

Alternative approaches to the development of an immunocompetent murine model of Ewing sarcoma have been ongoing, given the historical lack of a robust genetically engineered *in vivo* mouse model. Humanized murine models have been increasingly utilized to allow for the study of human adult carcinomas and testing of emerging immunotherapies in these cancers (67–69). Several different approaches exist for the development of a humanized murine model (70, 71). The Hu-PBL model utilizes direct infusion of mature human peripheral blood leucocytes (PBL) into immunodeficient (SCID) mice (70). The benefit of this model is the relative

Table 1. Published or commercially available Ewing sarcoma cell lines.

Name	Fusion status	Origin	Age (sex)	Disease stage	Genetic variants	Source	Year established (clinical outcome)
A-673	EWSR1-FLI1 fusion (ex7–ex6)	Muscle (primary)	15 (F)	Unknown	**TP53** (A119Qfs*5) homozygous; CDKN2A (c.1_471del471) homozygous; BRAF (V600E) heterozygous	ATCC, #CRL-1598 (PMID: 4357758 and 12606131)	1973
TC-71	EWSR1-FLI1 fusion (ex7–ex6)	Humerus (primary)	22 (M)	Relapse and metastatic (after treatment)	**TP53** (R213X and G245C); CDKN2A (homozygous deletion)	DSMZ, #ACC 516 (PMID: 3004699)	1981
TC-32	EWSR1-FLI1 fusion (ex7–ex6)	Ileum and adjacent soft tissue (primary)	17 (F)	Diagnosis (before treatment)	**STAG2** (Y636fs); CDKN2A (homozygous deletion)	COG (PMID: 3004699)	1979 (deceased)
CHLA-9	EWSR1-FLI1 fusion (ex7–ex6)	Thoracic mass (primary)	14 (F)	Diagnosis (before treatment)	**STAG2** (V628insTDI); CDKN2A (exonic loss)	COG (PMID: 15289350)	Unknown
CHLA-10	EWSR1-FLI1 fusion (ex7–ex6)	Thoracic lymph node (metastatic)	14 (F)	Relapse (after treatment)	**TP53**	COG (PMID: 15289350)	Unknown
CHLA-32	EWSR1-FLI1 fusion (ex7–ex6)	Pelvic (primary)	8.5 (F)	Diagnosis (before treatment)	**TP53** (R342X)	COG (PMID: 15289350)	Unknown
SK-N-MC	EWSR1-FLI1 fusion (ex7–ex6)	Retro-orbital metastasis (metastatic)	12 (F)	Relapse (after treatment)	**TP53** (expression loss)	ATCC #HTB-10; DSMZ, #ACC 203; PMID: 4748425, 8040301	1971
EW-7	EWSR1-FLI1 fusion (ex7–ex6)	Pleural effusion (metastatic)	20 (F)	Unknown	CDKN2A (deletion)	IARC (PMID: 6713356)	1982
EW-8 (Rh1)	EWSR1-FLI1 fusion (ex7–ex6)	Abdominal mass (primary)	17.8 (M)	Diagnosis (before treatment)	**STAG2** (N475fs); **TP53** (Y220C)	PPTP; DSMZ, #ACC 493 (PMID: 17154184)	Unknown
TC-244	EWSR1-FLI1 fusion (ex7–ex6)	Unknown	Unknown	Unknown	CDKN2A (homozygous deletion)	(PMID: 25010205)	Unknown
TC-248	EWSR1-FLI1 fusion (ex7–ex6)	Unknown	Unknown	Unknown	**TP53** (D259Y); CDKN2A (homozygous deletion)	(PMID: 9846984)	Unknown

(Continued on the following page)

Table 1. Published or commercially available Ewing sarcoma cell lines. (Cont'd)

Name	Fusion status	Origin	Age (sex)	Disease stage	Genetic variants	Source	Year established (clinical outcome)
TTC-547	EWSR1-FLI1 fusion (ex7–ex6)	Pelvis (primary)	13 (F)	Unknown	**TP53** (I263del); CDKN2A (homozygous deletion)	(PMID: 25010205)	Unknown
STA-ET-1	EWSR1-FLI1 fusion (ex7–ex6)	Humerus (primary)	13 (F)	Unknown	CDKN2A (homozygous deletion)	Prof. Heinrich Kovar, CCRI; PMID: 8378080	Unknown
POE	EWSR1-FLI1 fusion (ex7–ex6)	Unknown	Unknown	Unknown	**TP53** (L194R)	Institut Curie (PMID: 25010205)	Unknown
MIC	EWSR1-FLI1 fusion (ex7–ex6)	Unknown	Unknown	Unknown	**STAG2** (R216*); **TP53** (E285K)	Institut Curie (PMID: 25223734)	Unknown
EW-22	EWSR1-FLI1 fusion (ex7–ex6)	Unknown	Unknown	Unknown	**STAG2** (T463_L464fs); **TP53** (R175H)	Institut Curie (PMID: 25223734)	Unknown
EW-24	EWSR1-FLI1 fusion (ex7–ex6)	Unknown	Unknown	Unknown	**TP53** (K164E); PIK3CA (H1047R)	Institut Curie (PMID: 11423975)	Unknown
MS-EwS-15	EWSR1-FLI1 fusion (ex7–ex6)	Metastatic	Unknown (M)	Relapse	Unknown	University Children's Hospital Münster (PMID: 30879952)	Unknown
PSaRC219	EWSR1-FLI1 fusion (ex7–ex6)	Pleural fluid (metastatic)	Unknown (M)	Relapse	Unknown	University of Pittsburgh (PMID: 36658219)	2019
SBKMS-KS1 (SBSR-AKS)	EWSR1-FLI1 fusion (ex7–ex6)	Extraosseous inguinal lymph node (metastatic)	17 (F)	Unknown	Unknown	Technische Universität München (PMID: 19289832)	Unknown
SK-ES-1	EWSR1-FLI1 fusion (ex7–ex5)	Bone (primary)	18 (M)	Unknown	**STAG2** (Q735X); **TP53** (C176F)	ATCC, #HTB-86; DSMZ, #ACC 518; (PMID: 327080)	1971
RD-ES	EWSR1-FLI1 fusion (ex7–ex5)	Humerus (primary)	19 (M)	Unknown	**TP53** (R273C)	ATCC, #HTB-166; DSMZ, #ACC 260 (PMID: 8378080)	Unknown

(Continued on the following page)

Table 1. Published or commercially available Ewing sarcoma cell lines. (Cont'd)

Name	Fusion status	Origin	Age (sex)	Disease stage	Genetic variants	Source	Year established (clinical outcome)
SK-NEP-1	EWSR1-FLI1 fusion (ex7–ex5)	Pleural effusion (metastatic)	25 (F)	Relapse (after treatment)	**STAG2** (expression loss); **TP53** (G245S); CDKN2A (homozygous deletion)	ATCC, #HTB-48 (PMID: 17154184)	1971
ES-1	EWSR1-FLI1 fusion (ex7–ex5)	Left thigh (primary)	45 (F)	Diagnosis (before treatment)	**TP53** (R248Q); CDKN2A (homozygous deletion)	PPTP (PMID: 20164919)	Unknown
ES-4	EWSR1-FLI1 fusion (ex7–ex5)	Lung/pleura (primary)	18 (M)	Relapse	CDKN2A (homozygous deletion)	PPTP (PMID: 20164919)	Unknown
ES-8	EWSR1-FLI1 fusion (ex7–ex5)	Femur (primary)	10 (M)	Relapse	**STAG2** (5′ deletion); **TP53** (C135F); CDKN2A (homozygous deletion)	PPTP (PMID: 20164919)	Unknown
CHP100	EWSR1-FLI1 fusion (ex7–ex5)	Bone and spine (primary)	12 (F)	Unknown	**TP53** (H233fs)	Children's Hospital of Philadelphia; DSMZ, #ACC 830 (PMID: 10079, 33460449)	1972
6647	EWSR1-FLI1 fusion (ex7–ex5)	Pleural effusion (metastatic)	14 (F)	Relapse (after treatment)	**STAG2** (multi-exon deletion); **TP53** (S241F); CDKN2A (exonic loss); BRCA2 (S2186T)	(PMID: 327080)	1974
TC-215	EWSR1-FLI1 fusion (ex7–ex5)	Unknown	Unknown	Unknown	**STAG2** (tandem duplication); **TP53** (Y126C)	(PMID: 25010205)	Unknown
EW-1	EWSR1-FLI1 fusion (ex7–ex5)	Pleural effusion (metastatic)	19 (M)	Unknown	**TP53** (R273C); CDKN2A (deletion)	IARC; (PMID: 6713356)	1980
EW-2	EWSR1-FLI1 fusion (ex7–ex5)	Peripheral blood (circulating tumor cells)	19 (M)	Unknown	**TP53** (R273C)	IARC (PMID: 6713356)	1980
CHLA-258	EWSR1-FLI1 fusion (ex10–ex6)	Lung metastasis (metastatic)	14 (F)	Relapse (after treatment)	**TP53**; CDKN2A (homozygous deletion)	PPTP; COG (PMID: 15289350)	Unknown
ES-2	EWSR1-FLI1 fusion (ex10–ex6)	Ileum/bone marrow (metastatic)	14 (F)	Relapse	**STAG2** (E523X); **TP53** (R175H)	PPTP (PMID: 25010205)	Unknown

(Continued on the following page)

Table 1. Published or commercially available Ewing sarcoma cell lines. (Cont'd)

Name	Fusion status	Origin	Age (sex)	Disease stage	Genetic variants	Source	Year established (clinical outcome)
TC-240	EWSR1-FLI1 fusion (ex10–ex6)	Unknown	Unknown	Unknown	**STAG2** (R216X); **TP53** (R175H)	(PMID: 25010205)	Unknown
TC-253	EWSR1-FLI1 fusion (ex10–ex6)	Unknown	Unknown	Unknown	**STAG2** (N842fs); **TP53** (R273C)	(PMID: 25010205)	Unknown
PSaRC318	EWSR1-FLI1 fusion (ex10–ex6)	Lung (metastatic)	17 (M)	Relapse (after treatment)	BARD1 (E59Afs*8); CDKN2A and CDKN2B (deletion)	University of Pittsburgh (PMID: 36187937)	Unknown
ES-7	EWSR1-FLI1 fusion (ex10–ex5)	Right fibula/bone marrow (primary)	15 (M)	Relapse	**STAG2** (M1212fs); **TP53** (H179Q)	PPTP; (PMID: 20164919)	Unknown
TC-138	EWSR1-FLI1 fusion (ex10–ex5)	Bone (primary)	Unknown (M)	Unknown	**STAG2** (expression loss); CDKN2A (homozygous deletion)	(PMID: 25010205)	Unknown
ES-6	EWSR1-FLI1 fusion (ex9–ex4)	Right femur/rib/vertebra (primary)	17 (M)	Relapse	**STAG2** (L264P); **TP53** (expression loss)	PPTP (PMID: 20164919)	Unknown
EW-16	EWSR1-FLI1 fusion (ex8–ex7)	Unknown	Unknown (M)	Unknown	**TP53** (K120Sfs*3); CDKN2A (deletion)	Institut Curie (PMID: 11423975)	Unknown
SK-PN-DW	EWSR1-FLI1 fusion	Retroperitoneum (primary)	17 (M)	After chemo (after treatment)	**TP53** (C176F) homozygous; PTEN (c.1_79del79) homozygous; RB1 (W78*) homozygous	ATCC, #CRL-2139 (PMID: 3024811)	1978
EW-5	EWSR1-FLI1 fusion	Paraspinal (primary)	16.8 (M)	Diagnosis (after treatment)	**TP53**	PPTP (PMID: 31693904)	Unknown
EW-18	EWSR1-FLI1 fusion	Unknown	Unknown	Unknown	**TP53** (C176F)	IARC (PMID: 20164919)	Unknown
MHH-ES-1	EWSR1-FLI1 fusion	Bone (metastatic)	12 (M)	Unknown	**STAG2** (Q735fs); **TP53** (S215del)	DSMZ, #ACC 167 (DOI: 10.1016/0165-4608(89)90568-2)	Unknown
NCH-EWS1	EWSR1-FLI1 fusion	Lung (metastatic)	15 (M)	Relapse	Unknown	PPTP (PMID: 31927611)	Unknown
MS-EwS-6	EWSR1-FLI1 fusion	Thoracic cavity (metastatic)	19 (M)	Relapse	Unknown	University Children's Hospital Münster (PMID: 29464090)	Unknown
EWS-502	EWSR1-FLI1 fusion	Unknown	Unknown	Unknown	**TP53** (C135F)	(PMID: 23145994)	Unknown

(Continued on the following page)

Table 1. Published or commercially available Ewing sarcoma cell lines. (Cont'd)

Name	Fusion status	Origin	Age (sex)	Disease stage	Genetic variants	Source	Year established (clinical outcome)
CHLA-352 (COG-E-352)	EWSR1-ERG fusion (ex7–ex8)	Peripheral blood (circulating tumor cells)	17 (M)	Relapse (autopsy and after treatment)	**STAG2** (L791fs); **TP53** (R273H); CDKN2A (homozygous deletion)	COG (PMID: 24312454)	Unknown
CHLA-25	EWSR1-ERG fusion (ex7–ex7)	Unknown	2.6 (F)	After chemo (after treatment)	**STAG2** (multi-exon deletion); **TP53** (R273H)	COG (PMID: 24312454)	Unknown
SK-PN-LI	EWSR1-ERG fusion (ex7–ex7)	Right scapula (primary)	3 (M)	Unknown	**STAG2** (S704fs); **TP53** (R273H and V272L)	(PMID: 2987426)	1979
TC-106	EWSR1-ERG fusion (ex7–ex7)	Skin: scalp (metastatic)	19 (M)	Diagnosis (before treatment)	**TP53** (exonic splice site: E224D); CDKN2A (homozygous deletion); BRCA2 (K3326X)	(PMID: 3004699)	1982
TC-4C	EWSR1-ERG fusion (ex7–ex7)	Unknown	Unknown	Unknown	**STAG2** (multi-exon deletion); **TP53** (L194R)	(PMID: 25010205)	Unknown
CADO-ES1	EWSR1-ERG fusion	Pleural effusion (metastatic)	19 (F)	Unknown	CDKN2A (homozygous deletion)	DSMZ, #ACC 255 (PMID: 1756482)	Unknown (deceased)
EW-3	EWSR1-ERG fusion	Pleural effusion (metastatic)	14 (M)	Unknown	**STAG2** (R216*); **TP53** (c.852_858del7)	IARC; Institut Curie (PMID: 6713356)	1980
MS-EwS-34	EWSR1-ERG fusion	Bone marrow (metastatic)	10 (M)	Relapse	Unknown	University Children's Hospital Münster (PMID: 30879952)	Unknown

Comprehensive inventory of Ewing Sarcoma cell lines established from pediatric and young adult primary and metastatic tumors with associated mutations, source, and clinical information.
Abbreviations: CCRI, St. Anna Children's Cancer Research Institute; del, deletion; DSMZ, Leibniz Institute; ex, exon; F, female; fs, frameshift; IARC, International Agency for Research on Cancer; M, male.

accessibility of PBLs and the potential for paired PBLs with human tumor sample (autografted PBLs with Ewing sarcoma PDX). However, a significant limitation of this model is the relatively high rate of GVHD. Another humanized model is the bone marrow, liver, and thymus model. This model utilizes transplant of fetal liver $CD34^+$ progenitor cells and fetal thymus into immunodeficient mice (70). The benefit of the bone marrow, liver, and thymus model is that the implantation of human thymus material allows for HLA-restricted T-cell development and more robust development of T-cell populations. This model is limited by the availability of fetal tissues and is prone to the development of chronic GVHD. In contrast, the $CD34^+$ model utilizes infusion of $CD34^+$ stem cells, obtained from human cord blood, into an immunodeficient mouse (70). Total body irradiation is used for conditioning to prevent GVHD and allow for successful engraftment. The use of pre-conditioning in this model leads to exceedingly low rates of GVHD. The $CD34^+$ model allows for engraftment of all immune cell subpopulations, although relatively more limited myeloid and NK cell populations. It has been demonstrated that serotyping and aligning HLA-A*02 status is sufficient to prevent acute rejection in the setting of organ transplant and is true in humanized solid tumor cancer models as well (72, 73). Given this finding, it will be important that HLA-A*02 status is matched between Ewing sarcoma cell lines and $CD34^+$ cord blood donors when utilizing the $CD34^+$ humanized mouse model to prevent tumor rejection. As efforts to develop humanized mouse models continue to improve, it is expected that clinical efforts to minimize GVHD in humans may similarly be employed in mouse models to facilitate the engraftment and use of these models in preclinical studies (74, 75).

Studies investigating the Ewing sarcoma TME and agents targeting the TME using humanized mouse models are ongoing (76, 77). Previous work has demonstrated that Ewing sarcoma tumors utilizing the A673 cell line can be successfully established in NSG-SGM3 mice engrafted with $CD34^+$ cord blood stem cells (78). More recent work

has demonstrated that the study of Ewing sarcoma xenografts in the $CD34^+$ humanized mouse model leads to increased rates of spontaneous pulmonary metastases as compared with identical tumors developed in NSG mice (77). The use of humanized mouse models for *in vivo* studies of Ewing sarcoma is an emerging and important tool to study agents expected to affect or be affected by the tumor immune microenvironment, including immune checkpoint blockade and cellular therapies such as CAR-T.

PDX models

The development and use of immunodeficient mouse strains harboring xenografted tumor tissue have enabled insights into tumor biology and aided in the identification and evaluation of drugs that may be applicable to pediatric cancer (79, 80). Several efforts in establishing PDX mouse tumor models across the spectrum of pediatric cancer have resulted in an assembly of validated and biologically relevant models, which have become the gold standard for preclinical drug testing (81–85). PDX models are generally defined as models developed from direct implantation of patient tumor tissue into immunodeficient mice without prior culture or expansion *in vitro*, serially propagatable for at least two to three generations and recapitulate the molecular alterations of the source patient tumor. Recapitulation of tumor heterogeneity and gene alterations have made PDX models a unique biological surrogate of the patient and represent a unique and powerful tool for understanding and predicting drug responses. Drug responses in PDXs have been shown to correlate with clinical responses in a variety of co-clinical studies (79, 86–89). As such, there has been a shift from the use of xenografts established from cell lines expanded in *in vitro* culture, or cell line–derived xenografts (CDX), to PDXs for the evaluation and prioritization of drugs in the United States (85, 90). In Europe, the Innovative Therapies for Children with Cancer Pediatric Preclinical Proof-of-concept Platform (ITCC-P4; https://itccp4.com/) represents a sustainable, comprehensive preclinical drug-testing platform offering ~400 pediatric cancer PDX models, including 34 Ewing sarcoma models, which allow for the conduct of single-mouse co-clinical trials. A table of molecular and clinical characteristics of existing PDX models is summarized in **Table 2**.

Nonmammalian models

Nonmammalian models can also shed light on Ewing sarcoma biology and the function of EWS::FLI1 and related fusions. Zebrafish has proved to be a successful and tractable model of human Ewing sarcoma. Transgenic expression of human EWS::FLI1 in developing zebrafish led to the development of malignant round blue cell tumors with histologic and transcriptional activity similarity to human Ewing sarcoma (62). As with most GEMMs, this early zebrafish model was limited by developmental toxicity of the transgene, leading to low penetrance. Vasileva and colleagues (91) recently introduced an inducible model of EWS::FLI1 expression in zebrafish that overcame this limitation with rapid development of small round blue cell tumors at high penetrance. The tumors resemble human Ewing sarcoma at the histologic level and in the expression of canonical Ewing sarcoma markers such as CD99 and NKX2-2. Using this model, Vasileva and colleagues uncovered a novel role for heparan sulfate proteoglycans in tumor growth and showed that a heparan sulfate proteoglycan inhibitor decreased Ewing sarcoma tumorigenicity *in vitro* and *in vivo*. Zebrafish and humans share almost 85% of disease-causing genes, and the fish and human immune systems are highly similar, which will make this model a powerful platform for exploring biology and therapeutics of Ewing sarcoma.

More recent work from the same investigators showed that the expression of human EWS::FLI1 specifically in neural crest cells during early development leads to Ewing sarcoma tumors (bioRxiv 2024.10.27.620438). Single-cell analysis of RNA expression, chromatin accessibility, and EWS::FLI1 genomic binding demonstrated that EWS::FLI1 functions as an aberrant pioneer factor, hijacking developmental enhancers to reprogram neural crest cells to a mesoderm state. A striking manifestation of oncogenic reprogramming of neural crest to mesoderm is the formation of ectopic fins throughout the fish body. The association of neural crest–derived Ewing sarcoma with the fins of fish may also explain why human Ewing sarcomas are often found in bones of the limbs. These data provide an explanation for the mixed neuronal/mesenchymal nature of Ewing sarcoma cells and indicate that neural crest may be a cell of origin for human Ewing sarcoma.

Another, complementary, the use of the zebrafish system for preclinical modeling of Ewing sarcoma is the strategy of xenografting human cancer cells into zebrafish embryos and larvae (roughly day 1–day 7 of development). These early-life stages have several advantages. As adaptive immunity does not develop until after day 7, embryos and larvae readily tolerate human cell xenografts. Furthermore, each breeding pair can produce serval 100 transparent embryos per week, making it straightforward to generate and visualize large numbers of xenografted test subjects. Drug screening is simple to perform by adding test compounds to the water (92, 93). Using this system, Distel and colleagues have tested effects of YK-479, the TEAD inhibitor K-975, and allosteric C-terminal Hsp90 inhibitors against Ewing sarcoma (94). In another study in zebrafish, these investigators showed that Ewing sarcomas are sensitive to combination therapies targeting antiapoptotic proteins MCL-1 and BCL-XL, a finding they further confirmed in an Ewing sarcoma PDX mouse model and highlights the utility of zebrafish as a relevant preclinical drug screening tool (95).

In terms of a non-vertebrate model of Ewing sarcoma, Molnar and colleagues (96) used *Drosophila* to test the effects of EWS::FLI1 and discovered a natural spontaneous variant designated EWS::FLI1FS, in which the 69 amino acid C-terminal tail of the fusion is replaced by a new 64 amino acid sequence. The variant fusion was the only one tolerated by the developing fly salivary gland tissue. Surprisingly, multiomic analysis of the fly tissues showed enrichment of *EWSR1::FLI1*-related gene sets and pathways, including DNA replication, excision repair, and mismatch repair. Immunoprecipitation/mass spectrometry experiments demonstrated that *Drosophila* EWS::FLI1 interacts with the *Drosophila* homologues of human EWS::FLI1 protein partners, including RNA pol II subunits, chromatin remodelers, and components of the spliceosome. The *Drosophila* model recapitulates the major neomorphic aspects of the fusion oncogene function, i.e., activation of transcription from GGAA microsatellites and competition of ETS transcription factors. Most recent work by the same group has shown that EWS::FLI1FS lower toxicity is owed to reduced protein levels caused by its frameshifted C-terminal peptide (97). Using this knowledge, they have generated *Drosophila* lines that express full-length, unmodified EWS::FLI1 and described a positive linear correlation between the upregulation of transcription from GGAA microsatellites and a wide range of EWS::FLI1 protein concentrations. In contrast, GGAA microsatellite–independent transcriptomic dysregulation presents relatively minor differences across the same range. These results highlight the functional relevance of varying EWS::FLI1 expression levels and provide experimental tools to investigate in *Drosophila* the molecular

Table 2. Published Ewing sarcoma PDX models.

PDX ID	Fusion status	Diagnostic/ recurrent[a]	Treatment[b]	Site[c]	Age[d] (sex[e])	Previous treatment[f]	Other molecular alterations[g]	Related models	Center PDX developed
HSJD-ES-001	*EWSR1-FLI1* fusion (ex7–ex5)	R	After treatment	Scapula (P)	21.7 (M)	G/D, I/T, RT, and HIFU	STAG2 mutation		Hospital Sant Joan de Déu (PMID: 30140378)
HSJD-ES-002	*EWSR1-FLI1* fusion (ex10–ex5)	D	Before treatment	Fibula (P)	12.2 (M)	None	Two-copy gain of chr8 and focal deletion of the CDKN2A locus on chromosome 9p21.	PDX: HSJD-ES-006	Hospital Sant Joan de Déu (PMID: 29358035)
HSJD-ES-003	*EWSR1-FLI1* fusion (ex10–ex5)	R	After treatment	Lung (M)	17.0 (F)	GEIS21 (high risk)	Gain of chr8.		Hospital Sant Joan de Déu (PMID: 36603685)
HSJD-ES-004	*EWSR1-FLI1* fusion (ex7–ex6)	R	After treatment	Mediastinum (M)	18 (M)	SEHOP 2001	Gain of chr8 and loss in the locus encoding for CDKN2A. Wild type for STAG2 and TP53.		Hospital Sant Joan de Déu (PMID: 26056084)
HSJD-ES-006	*EWSR1-FLI1* fusion (ex10–ex5)	R	After treatment	Lung nodule (M)	13.7 (M)	GEIS21 (standard risk)	One-copy gain of chr8 and focal deletion of the CDKN2A locus on chromosome 9p21. Wild type for STAG2 and TP53.	PDX: HSJD-ES-002	Hospital Sant Joan de Déu (PMID: 26056084)
HSJD-ES-008	*EWSR1-FLI1* fusion (ex7–ex6)	D	Before treatment	Humerus (P)	13 (M)	None	Copy-neutral LOH in chromosome 3 and 20.	PDX: HSJD-ES-012	Hospital Sant Joan de Déu (PMID: 33837665)
HSJD-ES-009	*EWSR1-FLI1* fusion (ex7–ex5)	R	After treatment	Skull (M)	10.7 (M)	GEIS21 (standard risk)	Gain of chr8 and loss in the locus encoding for CDKN2A.		Hospital Sant Joan de Déu (PMID: 30420447)
HSJD-ES-011	*EWSR1-FLI1* fusion (ex7–ex6)	R	After treatment	Pleura (M)	13.9 (F)	SEHOP 2001, VIT	Gain of chr8.		Hospital Sant Joan de Déu (PMID: 30140378)
HSJD-ES-012	*EWSR1-FLI1* fusion (ex7–ex6)	R	After treatment	Skull (M)	14.7 (M)	GEIS21 (high risk); I/T; G/D	Copy-neutral LOH in chromosome 3p and 20q.	PDX: HSJD-ES-008	Hospital Sant Joan de Déu (PMID: 33669730)
HSJD-ES-013	*EWSR1-FLI1* fusion (ex7–ex6)	R	After treatment	Trapezius (M)	18.6 (M)	GEIS21 (standard risk)	CNAs in regions of chromosomes 8, 14, and 17 that include loss of TP53, STAT3, and BRAC1 genes.	PDX: HSJD-ES-017	Hospital Sant Joan de Déu (PMID: 33033246)
HSJD-ES-014	*EWSR1-FLI1* fusion	R	After treatment	Mastoid (M)	10.6 (M)	EuroEwing 2012	Gain of chr8 and loss in the locus encoding for CDKN2A.		Hospital Sant Joan de Déu (PMID: 36603685)
HSJD-ES-015	*EWSR1-FLI1* fusion (ex7–ex6)	R	After treatment	Lung (M)	18.3 (M)	GEIS21 (standard risk)	Gain of chr8.		Hospital Sant Joan de Déu (PMID: 33837665)
HSJD-ES-016	*EWSR1-FLI1* fusion (ex7–ex6)	R	After treatment	Lung (M)	12 (M)	GEIS21 (high risk)	Gain of chr8 and loss in the locus encoding for CDKN2A.		Hospital Sant Joan de Déu (PMID: 33669730)
HSJD-ES-017	*EWSR1-FLI1* fusion (ex7–ex6)	D	Before treatment	Pleura (P)	17.9 (M)	None	CNAs in chromosomes 7, 9, 10, 12, and 15 (involving the loss of CDKN2A locus).	PDX: HSJD-ES-013	Hospital Sant Joan de Déu (PMID: 33837665)
HSJD-ES-021	*EWSR1-FLI1* fusion (ex7–ex5)	R	After treatment	Paraspinal (M)	5.8 (F)	EuroEwing 2012	Unknown		Hospital Sant Joan de Déu (PMID: 36603685)
HSJD-ES-026	*EWSR1-FLI1* fusion	R	After treatment	Tibia (P)	14.8 (F)	EuroEwing 2012, G/D, I/T, and RT	Unknown		Hospital Sant Joan de Déu (PMID: 36603685)
HSJD-ES-033	*EWSR1-FLI1* fusion	R	After treatment	Lung (M)	9.3 (M)	GEIS21 (standard risk), G/D, I/T, and RT	Unknown		Hospital Sant Joan de Déu (PMID: 36603685)
IC-pPDX-3	*EWSR1-FLI1* fusion (ex7–ex6)	D	Before treatment	Humerus (P)	16 (F)		CDKN2A deletion		Institut Curie (PMID: 31668005)
IC-pPDX-5	*EWSR1-FLI1* fusion (ex7–ex6)	D	Before treatment	Tibia (P)			Unknown		Institut Curie (PMID: 32049009)

(Continued on the following page)

Table 2. Published Ewing sarcoma PDX models. (Cont'd)

PDX ID	Fusion status	Diagnostic/ recurrent[a]	Treatment[b]	Site[c]	Age[d] (sex[e])	Previous treatment[f]	Other molecular alterations[g]	Related models	Center PDX developed
IC-pPDX-8	*EWSR1-FLI1* fusion (ex10–ex8)	D	Before treatment	Sacrum (P)			STAG2 R614*		Institut Curie (PMID: 32049009)
IC-EW-1 (IC-pPDX-18)	*EWSR1-FLI1* fusion	R	After treatment	Retro-peritoneal pararenal (M)	5.2 (M)	CHX (Vc, If, and Ac; Dx, Et, and Cy)	STAG2 0.02 Mb homozygous deletion		Institut Curie (PMID: 37723198)
IC-pPDX-52	*EWSR1-FLI1* fusion (ex7–ex6)	D	Before treatment	Sacrum/ilium (P)			Unknown	PDX: IC-pPDX-87	Institut Curie (PMID: 32049009)
IC-pPDX-80	*EWSR1-FLI1* fusion (ex7–ex6)	D	After treatment	Chest (P)	8.2 (F)	CHX (Vc, If, Dx, Cy, Et, Ca, and Ac; Tz, Ir; Vb, Ce; CHIP)	Unknown		Institut Curie (PMID: 32049009)
IC-pPDX-87	*EWSR1-FLI1* fusion (ex7–ex6)	R	After treatment	Sacrum/ilium (P)	13.5 (M)	CHX (Vc, If, Dx, Cy, Et, Ac, and Zo)	TP53 R175C; RECQL4 p.Pro466Leu VP; TP53 LOH; and CDKN2A/2B homozygous deletion	PDX: IC-pPDX-52	Institut Curie (PMID: 32049009)
IC-EW-7 (IC-pPDX-141)	*EWSR1-FLI1* fusion	R	After treatment	Thoracic left (P)	13.3 (F)	CHX + RT (Vc, If, Dx, Cy, Et, and Ac)	Unknown		Institut Curie (PMID: 37723198)
IC-EW-8 (IC-pPDX-152)	*EWSR1-FLI1* fusion	R	After treatment	Lung (M)	7.1 (F)	CHX (Vc, If, Dx, Et, and Ac)	Unknown		Institut Curie (PMID: 37723198)
IC-EW-10 (IC-pPDX-164)	*EWSR1-FEV* fusion	R	After treatment	Vertebra Th11 (M)	18.0 (M)	CHX (Vc, If, Dx, Cy, and Et; Tz, Ir, and Vb)	TP53 p.Arg280Lys VP; TP53 LOH		Institut Curie (PMID: 35565457)
GR-EW-3	*EWSR1-FLI1* fusion	R	After treatment	Femur (P)	15.4 (M)	CHX (Vc, If, Dx, Cy, and Et)	TP53 p.Arg273Cys VP; TP53 LOH; CDK4 amplification (16 copies)		Gustave Roussy (PMID: 37723198)
GR-EW-5	*EWSR1-FLI1* fusion	R	After treatment	Lung (M)	15.3 (F)	CHX (Vc, If, Dx, Cy, Et, Ac, and Zo)	ARID2 p.Tyr1099GlyfsTer7 VP; CHEK1 deletion (1 copy)		Gustave Roussy (PMID: 37723198)
GR-EW-7	*EWSR1-FLI1* fusion	R	After treatment	Subperitoneal muscular (M)	18.3 (M)	CHX + RT (Vc, If, Dx, Cy, and Et; Tz, Ir; Me, Bu; Vb, Vr)	RAD54B p.Lys132Asn VUS; TOP2A p.Lys607ArgfsTer11 VP		Gustave Roussy (PMID: 37723198)
GR-EW-9	*EWSR1-FLI1* fusion	R	After treatment	Lung (M)	8.9 (M)	CHX (Vc, If, Dx, Cy, Et, and Ac; Tz, Ir)	Unknown		Gustave Roussy (PMID: 37723198)
GR-EW-10	*EWSR1-FLI1* fusion	R	After treatment	Lung (M)	23.6 (F)	CHX (Vc, If, Dx, Et; Tz, and Ir; Ac, Cy, and Vr)	Unknown		Gustave Roussy (PMID: 37723198)
GR-EW-11	*EWSR1-FLI1* fusion	R	After treatment	Arm right (M)	12.8 (F)	CHX (Vc, If, Dx, and Et)	TP53 p.Tyr197Cys VP; TP53 LOH		Gustave Roussy (PMID: 37723198)
NAN-EWS-2	*EWSR1-FLI1* fusion	R	After treatment	Scapula bone right (P)	6.6 (M)	CHX + RT (Vc, If, Dx, Cy, and Et; Me, Bu; Vb)	Unknown		Centre hospitalier universitaire de Nantes (PMID: 37723198)
VHIR-EW-2 (T761)	*EWSR1-FLI1* fusion	R	After treatment	Lung (M)	10.6 (F)	CHX (Vc, If, Dx, Cy, and Et)	STAG2 c.819+1G>A VP; FGFR1 p.Lys687Glu VP		Vall d'Hebron Research Institute (PMID: 37723198)
SJEWS001321_X1	*EWSR1-FLI1* fusion	D	After treatment	Tibia (P)	10 (M)	CHX	Unknown		St. Jude Children's Research Hospital (PMID: 28854174)
SJEWS030393_X1	*EWSR1-FLI1* fusion	R	After treatment	Lung (M)	17 (F)	CHX	Unknown		St. Jude Children's Research Hospital (PMID: 28854174)
SJEWS030565_X1	*EWSR1-FLI1* fusion	R	After treatment	Lung (M)	14 (F)	CHX	Unknown		St. Jude Children's Research Hospital (PMID: 28854174)
SJEWS031703_X1	*EWSR1-FLI1* fusion	D	After treatment	Pelvis (P)	15 (M)	CHX	Unknown		St. Jude Children's Research Hospital (PMID: 28854174)
SJEWS046144_X1	*EWSR1-FLI1* fusion	D	Before treatment	Chest wall (P)	15 (M)	None	Unknown		St. Jude Children's Research Hospital (PMID: 28854174)
SJEWS049193_X1	*EWSR1-FLI1* fusion	R	After treatment	Lung (M)	11 (M)	CHX	TP53 mutation		St. Jude Children's Research Hospital (PMID: 28854174)

(Continued on the following page)

Table 2. Published Ewing sarcoma PDX models. (Cont'd)

PDX ID	Fusion status	Diagnostic/ recurrent[a]	Treatment[b]	Site[c]	Age[d] (sex[e])	Previous treatment[f]	Other molecular alterations[g]	Related models	Center PDX developed
SJEWS049193_X2	*EWSR1-FLI1* fusion	R	After treatment	Lung (M)	11 (M)	CHX	Unknown		St. Jude Children's Research Hospital (PMID: 28854174)
SJEWS056156_X1	*EWSR1-FLI1* fusion	R	After treatment	Rib (M)	22 (M)	CHX	Unknown		St. Jude Children's Research Hospital (PMID: 28854174)
SJEWS056156_X2	*EWSR1-FLI1* fusion	R	After treatment	Rib (M)	22 (M)	CHX	Unknown		St. Jude Children's Research Hospital (PMID: 28854174)
SJEWS063826_X1	*EWSR1-FLI1* fusion	R		Axilla	17 (M)		Unknown		St. Jude Children's Research Hospital (PMID: 28854174)
SJEWS063834_X1	*EWSR1-FLI1* fusion	R		Chest wall	14 (F)		Unknown		St. Jude Children's Research Hospital (PMID: 28854174)
SJEWS063829_X1	*EWSR1-FLI1* fusion	D	After treatment	Femur (P)	8 (F)	CHX	Unknown		St. Jude Children's Research Hospital (PMID: 28854174)
SJEWS063834_X2	*EWSR1-FLI1* fusion	R		Lung (M)	14 (F)		Unknown		St. Jude Children's Research Hospital (PMID: 28854174)
SJEWS071780_X1	*EWSR1-FLI1* fusion	D	After treatment	Chest wall (P)	18 (F)	CHX	Unknown		St. Jude Children's Research Hospital (PMID: 28854174)
SJEWS071783_X1	*EWSR1-FLI1* fusion	R	After treatment	Chest	20 (M)	CHX	Unknown		St. Jude Children's Research Hospital (PMID: 28854174)
SJEWS071783_X2	*EWSR1-FLI1* fusion	R	After treatment	Lung (M)	20 (M)	CHX	Unknown		St. Jude Children's Research Hospital (PMID: 28854174)
SJEWS071783_X3	*EWSR1-FLI1* fusion	R	After treatment	Lung (M)	20 (M)	CHX	Unknown		St. Jude Children's Research Hospital (PMID: 28854174)
SJEWS071783_X4	*EWSR1-FLI1* fusion	R	After treatment	Spleen	20 (M)	CHX	Unknown		St. Jude Children's Research Hospital (PMID: 28854174)
SJEWS071785_X1	*EWSR1-FLI1* fusion	R	After treatment	Spine	12 (F)	CHX	Unknown		St. Jude Children's Research Hospital (PMID: 28854174)
SJEWS071783_X5	*EWSR1-FLI1* fusion	R	After treatment	Liver (M)	20 (M)	CHX	Unknown		St. Jude Children's Research Hospital (PMID: 28854174)
SJEWS071785_X2	*EWSR1-FLI1* fusion	R	After treatment	Periorbital (M)	12 (F)	CHX	Unknown		St. Jude Children's Research Hospital (PMID: 28854174)
TCCC-EWS37	*EWSR1-FLI1* fusion		Before treatment	Unknown	9 (M)	None	Unknown		Baylor College of Medicine, Houston (PMID: 30548185)
TCCC-EWS38	*EWSR1-FLI1* fusion		Before treatment	(P)	12 (M)	None	Unknown		Baylor College of Medicine, Houston (PMID: 30548185)
TCCC-EWS70	*EWSR1-FLI1* fusion		Before treatment	(P)	12 (M)	None	Unknown		Baylor College of Medicine, Houston (PMID: 30548185)
TCCC-EWS82	*EWSR1-FLI1* fusion		Before treatment	Unknown	14 (F)	None	Unknown		Baylor College of Medicine, Houston (PMID: 30548185)
EW#1	*EWSR1-FLI1* fusion (ex7–ex6)		After treatment	Lung (M)	49 (F)	CHX	Wild-type TP53		IRCCS Istituto Ortopedico Rizzoli (PMID: 31434953)
EW#2	*EWSR1-FLI1* fusion (complex type)	R	Before treatment	Shoulder and soft tissue (P)	28 (M)	None	Wild-type TP53		IRCCS Istituto Ortopedico Rizzoli (PMID: 31434953)
EW#3	*EWSR1-ERG* fusion		After treatment	(P)	14 (M)	CHX	Wild-type TP53		IRCCS Istituto Ortopedico Rizzoli (PMID: 31434953)

(Continued on the following page)

Table 2. Published Ewing sarcoma PDX models. (Cont'd)

PDX ID	Fusion status	Diagnostic/ recurrent[a]	Treatment[b]	Site[c]	Age[d] (sex[e])	Previous treatment[f]	Other molecular alterations[g]	Related models	Center PDX developed
EW#4	*EWSR1-FLI1* fusion (ex7–ex6)		After treatment	Pelvis (P)	17 (F)	CHX	Wild-type TP53		IRCCS Istituto Ortopedico Rizzoli (PMID: 31434953)
EW#5	*EWSR1-FLI1* fusion (ex7–ex5)		After treatment	Femur (P)	25 (M)	CHX	Wild-type TP53		IRCCS Istituto Ortopedico Rizzoli (PMID: 31434953)
EW#6	*EWSR1-FLI1* fusion (ex7–ex6)		After treatment	(P)	7 (F)	CHX	Unknown		IRCCS Istituto Ortopedico Rizzoli (PMID: 31434953)
XEN-EWS-021	*EWSR1-FLI1* fusion	D	After treatment	Spine (M)	18 (F)	Single dose of Dx/Cy prior to excision	STAG2 mutation (<50% variant allele frequency); p53 homozygous mutation		NCI, Bethesda (PMID: 27608846)

[a]Diagnostic/recurrent: Diagnostic (D) refers to samples obtained during the initial treatment period including those obtained prior to therapy as well as after initial preoperative chemotherapy. Recurrent (R) refers to samples obtained after the initial treatment period at a time of disease recurrence.
[b]Treatment: Yes (Y) refers to patients who received some form of therapy within 1 month of sample acquisition. No (*N*) refers to patients who did not receive any therapy within 1 month of sample acquisition.
[c]Site: refers to the site that the sample was acquired from the patient. Primary site (P) and metastatic sample site (M) are noted.
[d]Age: refers to the age of the patient at the time of sample acquisition.
[e]Sex: male (M) or female (F).
[f]Previous treatment: Ac, actinomycine; Bu, busulfan; Ca, carboplatin; Ce, celecoxib; CHIP, mitomycine, cisplatin, and irinotecan; CHX, chemotherapy; CNA, copy-number alteration; Cy, cyclophosphamide; Dx, doxorubicin; Et, etoposide; G/D, clinical protocol including gemcitabine and docetaxel; GEIS21 (high risk), clinical protocol including G/D window phase, followed by five cycles of mP6 chemotherapy; surgery; RT; followed by G/D maintenance therapy; GEIS21 (standard risk), clinical protocol including five cycles of mP6 chemotherapy (cycles 1, 2, and 4 with cyclophosphamide, doxorubicin, and vincristine; and cycles 3 and 5 with ifosfamide and etoposide); surgery; radiation therapy; HIFU, high intensity focused ultrasound; I/T, clinical protocol including irinotecan and temozolamide; If, ifosfamide; Ir, irinotecan; Me, melphalan; RT, radiotherapy; SEHOP 2001, clinical protocol including six cycles of VIDE chemotherapy (day 1 vincristine, followed by days 1–3 with doxorubicin, ifosfamide, and etoposide); Tz, temozolomide; Vb, vinblastine; Vc, vincristine; VIT, clinical protocol including vincristine, irinotecan, and temozolomide; VP, phenotypic variance; Vr, vinorelbine; VUN, variant of uncertain significance; Zo, zoledronic acid.
[g]Other molecular alterations: copy-number alteration, loss of heterozygosity, phenotypic variance, and variant of uncertain significance.

pathways affected by the EWS::FLI1 "high" and "low" states observed in human tumors (97).

Descriptions of *in vitro* and *in vivo* models, pros and cons of their use in experiments, and model considerations are summarized in **Fig. 1**.

Preclinical Data Resources

In concert with the development of preclinical models, several informatics platforms have been assembled to catalogue and house molecular characterization data from primarily mouse xenograft models. Models generated by the NCI Pediatric Preclinical Testing Program (PPTP)/Pediatric Preclinical Testing Consortium (PPTC)/Pediatric *In VivO* Testing (PIVOT) preclinical testing groups have housed model data into the Patient Derived Cancer Models Database that contains information about each mouse model in addition to demographic and clinical characteristics of the source patient (https://www.cancermodels.org; ref. 98). Additionally, the Treehouse Childhood Cancer Initiative has developed an accessible database of pediatric patient tumors and PDX models with associated clinical, demographic, and model characterization data (https://treehousegenomics.ucsc.edu/). Although not specifically a repository for pediatric-specific models, the PDX Network Portal houses patient tumor and PDX data across a wide range of tumor types (https://portal.pdxnetwork.org/; ref. 99). Efforts to assemble legacy preclinical testing data conducted by the PPTP/PPTC/PIVOT group are underway to enable access of drug efficacy data to external investigators (http://preclinicalpivot.org). Similarly, the ITCC-P4 consortium, described in more detail in subsequent sections, has developed an open access platform containing searchable data on models and drug testing data (https://r2-itcc-p4.amc.nl/). PDX models generated by Cancer Prevention and Research Institute of Texas investigators have housed model information, pathology images, and an array of omics data into the Pediatric PDX Explorer platform, a searchable database that incorporates functionalities that enable online analysis (https://datacommons.swmed.edu/cce/ppdxe/data.php; ref. 100). The St Jude Pediatric Cancer portal includes *in vitro* and *in vivo* model–associated data for solid (https://cstn.stjude.cloud) and liquid tumors (https://propel.stjude.cloud; ref. 101). Using the cBioPortal platform, the PedcBioPortal was developed to house omics data from >200 preclinical models developed by the PPTP/PPTC group and is also linked to other pediatric cancer genomics initiatives such as NCI TARGET (https://pedcbioportal.org; ref. 81). There is ongoing efforts through the NCI Childhood Cancer Data Initiative to connect preclinical model data with patient demographic and genomic data obtained across a continuum of pediatric clinical studies (https://ccdi.cancer.gov/explore), as well as the related NCI Genomic Data Commons which houses pediatric patient genomics data (https://portal.gdc.cancer.gov; refs. 102, 103). These resources serve as invaluable data repositories to guide model selection for preclinical studies, as well as a minable resource to enable hypothesis-driven studies (**Table 3**).

The data produced by modern sequencing instruments is highly amenable to sharing, reuse, and continuous reanalysis. Unlike earlier generations of genomic and transcriptomic technologies, massively parallel sequencing methods produce data that have less "batch effects." This is a particular benefit for rare tumors, like Ewing sarcoma, for which multiple groups may want to combine locally produced data into a larger unified cohort. In these instances, raw sequence–level reads (BAM, CRAM, or FASTQ) may be shared

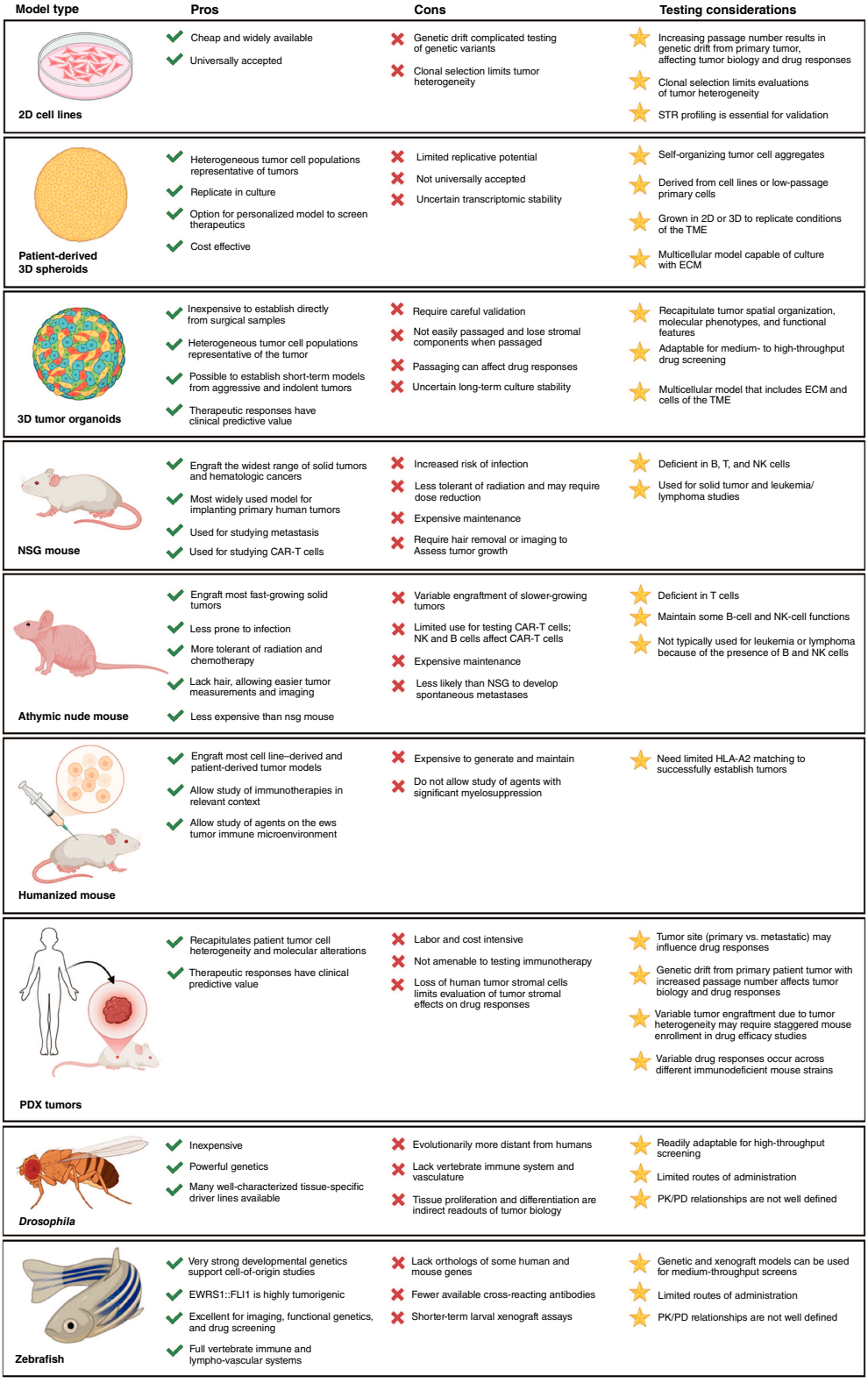

Figure 1.

Advantages and disadvantages of Ewing sarcoma (EwS) preclinical models. Summary of preclinical models with associated pros and cons for each model type. Testing considerations for each model type are provided.

Table 3. Databases for pediatric cancers and preclinical models.

Database	Data resources	Data address	Reference
Patient Derived Cancer Models Database	PDX model characterization data	https://www.cancermodels.org	(86)
Treehouse Childhood Cancer Initiative	Clinical and PDX genomics data	https://treehousegenomics.ucsc.edu/	
PDX Network Portal (PDXNet)	Clinical and PDX genomics data	https://portal.pdxnetwork.org/	(87)
PIVOT Data Portal	PDX model and drug efficacy study data	http://preclinicalpivot.org	
ITCC-P4 R2 Genomics Analysis & Visualization Platform	Clinical and PDX genomics data	https://r2-itcc-p4.amc.nl/	
Pediatric PDX Explorer	Clinical and PDX genomics data	https://datacommons.swmed.edu/cce/ppdxe/data.php	(88)
St Jude PeCan Cloud Models Portal	Clinical and PDX genomics data	https://cstn.stjude.cloud	(89)
PedcBioPortal	Clinical and PDX genomics data	https://pedcbioportal.org	(69)
NCI Childhood Cancer Data Initiative	Clinical and genomics data	https://ccdi.cancer.gov/explore	(90)
NCI Genomic Data Commons	Clinical and genomics data	https://portal.gdc.cancer.gov	(91)

or, alternatively, processed variants or summarized gene counts, so long as similar library preparation methods and standardized bioinformatics pipelines are used at all sites. For instance, an analysis of structural rearrangements in Ewing sarcoma led to the identification of a pattern of looped translocations called chromoplexy, involving *EWSR1*, *FLI1*, *ERG* and additional loci (104). A data reanalysis of additional Ewing sarcoma genomes, sequenced elsewhere, led to the validation of this pattern.

Data reanalysis and sharing have also been useful for full transcriptome data [RNA sequencing (RNA-seq)]. The Ewing sarcoma transcriptome is highly complex and its analysis benefits from large sample sizes. The UCSC Treehouse initiative has assembled a uniformly processed set of 12,747 cancer transcriptomes, which includes 80 samples marked as Ewing sarcoma (105). Combining this dataset with RNA generated elsewhere, a pan-cancer atlas of human cancer was developed (106). The atlas was built using a scale-adaptive unsupervised approach that led to an initial set of 455 distinct classes of cancer and non-neoplastic tissue. Ewing sarcoma clustered distinctly from all other cancers, including other mesenchymal entities, in a clearly distinguished class. Notably, this class contained only FET::ETS fusions and clarified the diagnosis of tumors previously diagnosed as Ewing sarcoma that harbored other fusions. A convolutional neural network (OTTER) was then trained on these classes and made available online (https://otter.ccm.sickkids.ca/). This facilitated matching of locally sequenced RNA-seq to a large atlas, helping to refine diagnosis for newly diagnosed patients. This system also enables an objective evaluation of the degree to which models of Ewing sarcoma recapitulate human disease *in situ*. The same approach can be used to assess the degree to which experimental perturbations influence the overall transcriptional signature in models.

In vivo Drug Efficacy Studies

Given poor outcomes for patients with metastatic or relapsed/refractory disease, there is an urgent need to identify new therapeutic strategies and streamline preclinical testing and translation to benefit high-risk patients (107, 108). There has been considerable preclinical work both in optimizing delivery of chemotherapeutic regimens used in the upfront and relapsed setting, as well as investigation of novel therapeutics such as small-molecule inhibitors and immunotherapy in animal models. Here, we describe some of the efforts thus far and discuss key recommendations for future *in vivo* preclinical testing.

Establishment of chemotherapy backbones *in vivo*

As chemotherapy regimens remain the standard of treatment in both upfront and relapsed disease in patients, efforts have focused on optimization of chemotherapy regimens using *in vivo* models. Work from the early-phase preclinical pharmacology program at St. Jude has established mouse *in vivo* dosing and scheduling with accompanying pharmacokinetic data of standard chemotherapy regimens and many small-molecule inhibitors (https://cstn-gateway-prod.azurewebsites.net/p/pdfs/Standard_Of_Care_Drug_Regimens.pdf and https://cstn.stjude.cloud/resources#pkreports). Although many novel therapeutics have emerged and shown promising preclinical results, the use of single agents is unlikely to result in significant therapeutic benefit in the clinic. We currently lack a complete understanding of how Ewing sarcoma cells resist standard chemotherapy and focused efforts to measure dynamic changes and targets serially in the context of how chemotherapy would aid translation of therapies to clinical trials. Thus, a priority for future preclinical studies will be testing combinations of backbone chemotherapeutic agents with novel therapeutics.

Modeling transcriptional heterogeneity and plasticity in therapeutic studies

Despite the characteristic "quiet genome" of Ewing sarcoma, Ewing sarcoma tumors exhibit profound transcriptional and epigenetic heterogeneity. In particular, the EWS::FLI1 fusion regulates the expression of both neural and mesenchymal transcriptional profiles through complex transcriptional and epigenetic mechanisms (53–55). Moreover, Ewing sarcoma cells are highly plastic and exhibit profound transcriptional and phenotypic state heterogeneity that is controlled by both cell-intrinsic and cell-extrinsic signals (109). In particular, the relative expression level and transcriptional activity of the EWS::FLI1 fusion and the TME, respectively, are key determinants of cell state (10, 110–112). Ewing sarcoma cell proliferation requires an optimal EWS::FLI1 protein threshold, frequently referred to as EWS::FLI1 "high" state, whereas relatively reduced EWS::FLI1 concentrations at the EWS::FLI1 "low" state were found associated with a mesenchymal migratory and invasive phenotype (10). Fluctuations between these two cell states have been proposed to drive Ewing sarcoma metastasis (10). There is

increasing evidence that these altered states contribute to therapeutic response and resistance and that drug treatment itself can further influence this plasticity (113, 114). To advance therapeutics for high-risk patients, it is essential to design preclinical studies that investigate both treatment effect and response in the context of cellular plasticity.

Two recent publications model this transcriptional heterogeneity in *in vivo* models. Recent spatial transcriptomic analysis of Ewing sarcoma models revealed marked spatial differences in gene expression between tail vein–derived and subcutaneous tumors (115). In addition, marked intratumoral heterogeneity of transcriptomic and phenotypic states was observed in these models. Notably, protumorigenic ECM gene programs were enriched in cells in invasive foci and along tumor border adjacent to tumor stroma (115). Many of these ECM-enriched signatures recapitulate the EWS::FLI1 "low" state phenotypically and transcriptionally and these ECM-secreting tumor cells were also regionally identified in patient tumor biopsies. In further support of this, Dasgupta and colleagues (116) evaluated the transcriptional programs of spontaneous lung metastases that formed following serial orthotopic intratibial injection and showed that metastatic tumors had transcriptional profiles distinct from parent cells. Significantly, and consistent with studies above, the signatures of these metastatic cells showed enrichment of ECM and epithelial–mesenchymal transition gene signatures. Moreover, similar genes were upregulated in lung metastases isolated from patients (116). These studies together demonstrate that phenotypic heterogeneity of tumor cells is inherent to the biology of Ewing sarcoma and is evident during tumor evolution and metastatic progression in patient tumors *in vivo*. Given that targeted and cytotoxic drugs can have differential effects on tumor cells in different states, it will be critical that these important biological features be considered in the development of novel therapeutic regimens.

Modeling considerations for *in vivo* preclinical testing

As we design future preclinical therapeutic studies, we provide recommendations and considerations for *in vivo* model selection to ensure biologically rational testing of therapeutics. When selecting a model for preclinical studies, investigators should consider key validation criteria, including confirmation of the *EWSR1::FLI1* fusion and other defining mutations (via STR profiling or sequencing), transcriptomic fidelity to primary Ewing sarcoma tumors, and preservation of histologic features. *In vivo* performance parameters such as engraftment rate, metastatic potential, and treatment response should also be evaluated. Importantly, the model's relevance to the clinical context—whether newly diagnosed, relapsed, metastatic, or specific molecular subtypes—should guide its application. These considerations help ensure that model selection aligns with the intended research question and enhances translational relevance.

Tumor establishment can be accomplished via intratibial (orthotopic modeling), subcutaneous (heterotopic modeling), or tail vein injection (metastatic modeling), as well as a spontaneous metastatic model (amputation model). Each model is hypothesized to provide strengths and weaknesses for therapeutic discovery and translation. For example, intratibial or intrafemoral tumors have cross-talk with the bone TME, whereas spontaneous metastatic or disseminated tail vein injection may more reliably recapitulate tumor initiation in a metastatic niche. One focus is on the development of drugs that target and prevent formation of tumors in the metastatic setting, such as inhibitors of TGFβ and Wnt/β-catenin pathways. Nuclear translocation of β-catenin in Ewing sarcoma alters the actin cytoskeleton to increase migration/invasion, and pharmacologic inhibition of canonical Wnt signaling prevented metastatic lung colonization in a spontaneous metastasis model (117–119). Thus, testing of agents that block these important signals in metastatic niches should be performed in relevant models i.e., spontaneous metastasis or tail vein models rather than subcutaneous tumor models.

Alternative platforms have emerged to interrogate Ewing sarcoma metastasis. The Pulmonary Metastasis Assay is an *ex vivo* approach using precision-cut lung slices from immunodeficient mice that allows direct visualization of tumor cell colonization within the lung microenvironment (120). This system preserves tissue architecture and enables pharmacologic manipulation while reducing animal usage. Zebrafish xenograft models also support real-time, high-throughput evaluation of Ewing sarcoma cell migration, intravasation, and metastatic spread. Owing to the transparency and genetic conservation of zebrafish embryos, these models are especially valuable for rapid screening of metastasis-modulating agents (94, 121). Together, these platforms offer complementary tools to better understand Ewing sarcoma dissemination and therapeutic vulnerabilities beyond conventional murine systems.

An important consideration when developing *in vivo* models using CDX or PDX is the location of implantation. Most studies using *in vivo* models of Ewing sarcoma, especially those looking for preclinical efficacy of novel drugs, involve subcutaneous injections of cells suspended in Matrigel or PBS or involve subcutaneous implantation of fragments of tumors (either CDX or PDX). Subcutaneous tumors are technically simple to grow and easy to measure using calipers, thus facilitating large studies of drug efficacy. This is the approach generally adopted by the PPTP/PPTC/PIVOT programs (122). With the growing recognition of the importance of nonmalignant cells in the TME on the behavior of cancer, orthotopic tumor implantation approaches have been gaining traction. The main approaches taken in Ewing sarcoma are intratibial injection, implantation of tumor fragments into the pretibial space, and renal subcapsular implantation. It is becoming increasingly clear that the behavior of tumors depends significantly upon the location of implantation. One significant difference between subcutaneous tumors and tumors growing in an orthotopic location is the influence of microenvironment on metastatic behavior. One of the earliest studies directly comparing the behavior of xenografted tumors implanted subcutaneously with the same tumors implanted in the pretibial space was conducted by Goldstein and colleagues (123). In that study, which included two Ewing sarcoma PDX models and one cell line model, no distant metastases were observed in 45 mice subcutaneously implanted with a xenograft fragment, whereas 27% to 67% of mice (depending on the model) exhibited some evidence of distant metastasis after orthotopic implantation. Although not formally studied in Ewing sarcoma, a recent study of osteosarcoma demonstrated differences in response to doxorubicin between intra-osseous tumors and intramuscular tumors (124). These studies provide support for the use of orthotopic implantation models of Ewing sarcoma (and other sarcomas) despite the increased technical difficulty of these approaches because the interactions between tumor cells and the local microenvironment affect all aspects of tumor biology and cannot be appropriately modeled in the subcutaneous space.

Other groups have developed orthotopic models utilizing intratibial or intrafemoral injection of single-cell suspensions, which can be derived from cell lines or from PDX models. These models are

probably appropriate for the study of localized tumors and their response to various treatments because they mimic the interactions between tumor cells and normal bone. This was well demonstrated by Vormoor and colleagues (125) who used advanced imaging techniques, including PET and MRI, to define the interactions between tumors grown after intrafemoral injection of bone sarcoma cells and the surrounding normal bone. Nevertheless, although mice injected with sarcoma cells via the intratibial or intrafemoral approach develop distant metastases, this approach may not adequately model the entire metastatic cascade. Although not formally studied in Ewing sarcoma, Maloney and colleagues (126) demonstrated that within 30 minutes of intratibial injection of osteosarcoma cells, lungs are already seeded with cancer cells, suggesting that intratibial injection, like tail vein injection, simply seeds cells into the vasculature, rather than recapitulating the entire process of metastasis.

Renal subcapsular injections and injections into muscle have also been used to study Ewing sarcoma growth and progression. Although metastasis can develop after such implantations, the crucial interactions between tumor cells and the normal constituents of the Ewing sarcoma microenvironment (e.g., bone, soft tissue, and lung) cannot be studied in these models (127, 128).

In addition to using relapse-derived models, resistance can also be modeled through experimental induction. Serial passaging of xenografts under chemotherapy exposure or cyclic treatment protocols can enrich for resistant subpopulations while preserving tumor histology and molecular features. Such strategies have been applied in other sarcomas and offer a practical route to develop relapse-relevant models for preclinical testing (82, 83).

A major limitation of all mentioned models is the inability to study the interactions between cancer cells and the immune system as all these models rely on immune-deficient mice. Of course, not all immune-deficient mice are the same and different strains have different complements of immune cells that can interact with implanted tumor fragments. The use of different models with varying degrees of immune deficiency allows investigators to address some elements of the influence of the immune system on metastasis. Interestingly, the articles cited earlier in this section used a wide variety of mouse strains, including NSG mice (123, 125), Rag2/γc knockout mice (125), athymic nude mice (127), and NOD-SCID mice (128), which at least supports the contention that any of these strains can be used for modeling tumor/immune system interactions. The newest models being developed focus on so-called humanized mice, as described in more detail earlier in this review. These approaches, if combined with orthotopic implantation to ensure an appropriate microenvironment, have the potential to propel forward our understanding of tumor–immune interactions and of spontaneous distant metastasis by more accurately capturing all of the elements that affect tumor behavior in patients (77, 78).

Several high-profile examples in Ewing sarcoma highlight how preclinical findings, especially from CDX or subcutaneous PDX models, have failed to predict clinical outcomes. Insulin-like growth factor 1 receptor and PARP inhibitors both showed strong preclinical efficacy but limited clinical benefit, due in part to non-representative models, lack of metastasis or resistance features, and preclinical dosing that did not reflect clinical pharmacokinetics (129–131). Preclinical studies performed by the PPTC/PIVOT consortium reinforce the importance of using pharmacokinetically informed dosing, clinically relevant drug exposures, and modeling of relapse or metastasis to improve translational success (82). These lessons emphasize the need for more rigorous, context-aware study design to guide clinical prioritization.

In vivo drug efficacy study designs

Conventional drug efficacy studies in mouse xenograft models typically enroll five to 10 mice into each treatment arm and subsequent comparisons of tumor growth differences to assess treatment response. Although this approach can be used to evaluate the activity of a small number of drugs, it is not a feasible study design for larger numbers of agents or drug combinations. To address the challenge of an ever-increasing number of drugs and/or drug targets to be tested utilizing PDX models, the development of alternative preclinical study designs, such as the single mouse trial ($n = 1$ mouse per PDX model per drug), twin mouse trial ($n = 2$ mice per treatment arm per PDX model), or adaptive trial study designs (two-stage mouse enrollment strategy based on response from an initial cohort of $n = 3$ mice per treatment arm per PDX model) is required to enable testing of multiple drugs across multiple PDX models while decreasing mouse utilization required for testing (132, 133). Furthermore, metrics for assessing the antitumor activity of drugs or drug combinations include assessments of tumor volume change over time or at a predetermined timepoint and comparison of event-free survival utilizing tumor volume relative to baseline thresholds (e.g., doubling or quadrupling in tumor volume relative to baseline) as study endpoints (122, 134). Various recommendations for experimental study design and assessments of antitumor activity using PDX models have been developed, including consensus recommendations developed by the NCI PDX Development and Trial Centers Research Network (122, 133–136). Assessment of antitumor activity using two or more response metrics (e.g., comparisons of tumor volume changes and event-free survival) and tumor responses resulting in tumor regression or prolonged growth inhibition (stable disease) are generally considered to be more compelling for further investigation than treatments with statistically significant differences in tumor growth but in the setting of ongoing growth within the treatment group.t

North American and European Collaborative Preclinical Testing Efforts

In 2001, a workshop organized by the NCI and the COG identified the need for establishing a mechanism to evaluate and prioritize drugs for pediatric cancer (137). This meeting laid the foundation for the establishment of the NCI-sponsored PPTP in 2003, which incorporated *in vitro* cell lines and primarily CDX models in preclinical drug testing (122). Standards for defining drug responses in xenograft models have been developed to allow assessments of drug activity, which have been helpful in guiding drug comparisons and selection for translation into human clinical trials (122, 134). The PPTP has since undergone several iterations as the PPTC in 2015, which shifted to the standard use of primarily PDX models in preclinical testing, and most recently PIVOT in 2021, which expanded the number of testing sites from five to seven centers, with each center specializing in testing on particular tumor histologies. Enactment of the RACE for Children Act in 2020, which mandated pharmaceutical companies to evaluate drugs for pediatric cancer if a drug targets a protein "relevant to the growth or progression of a pediatric cancer," resulted in an increase in the

number of drugs requiring evaluation and prioritization for pediatric cancer (138, 139). Additional preclinical testing groups within the United States, such as the Pediatric Research in Oncology Xenografting Consortium, along with efforts in Europe through the EEC New Ewing Therapeutics Strategy group and the ITCC-P4, have been established to provide data critical for drug prioritization in pediatric cancer (140, 141).

In the frame of the IMI Innovative Medicine Initiative, the EU funded the ITCC-P4 (www.itccp4.eu) consortium in 2018, which associated academic and industrial partners with the goal of developing a large-scale PDX platform representing more than 400 high-risk pediatric cancers. This collection of PDX models includes 34 Ewing sarcoma PDX models generated either from primary ($n = 17$) or relapse ($n = 17$) disease. All PDXs had comprehensive molecular characterization (whole-exome and low-coverage whole-genome sequencing, DNA methylation profiling, and RNA-seq and gene expression profiling), as well as their matched human tumors and germline samples. All processed molecular and drug-testing data are collected in the consortium's centralized data repository (https://r2-itcc-p4.amc.nl/), allowing data downstream analysis, visualization, and interpretation. For sustainability of this platform, this comprehensive repertoire of modern laboratory models of pediatric tumors is now available to pharmaceutical companies and academic institutions for drug testing in the frame of the non-for-profit ITCC-P4 gGmbH. The aim is to systematically test new treatment options for children and adolescents with cancer and to contribute data to regulatory approval processes to make the development of new cancer therapies for children and adolescents more attractive for pharmaceutical companies and academic research institutions. The founding partners of the new ITCC-P4 gGmbH are several high-profile research institutions and biotech companies across Europe.

Notable international collaboration efforts relevant to Ewing sarcoma include recent efforts from the ACCELERATE Paediatric Strategy Forum which, in 2023, discussed the role of the DNA damage response pathway (DDR) and its inhibitors in Ewing sarcoma. Investigators extensively reviewed relevant biology and rationale of the DDR and DDR inhibitors in Ewing sarcoma and other pediatric cancers, preclinical testing, and the development of DDR inhibitors as part of pediatric investigation plans with the FDA–such as talazoparib in combination with liposomal irinotecan for relapsed/refractory Ewing sarcoma (142).

A Pediatric Molecular Targets List has been developed to catalog proteins relevant to pediatric cancer and provide industry collaborators with pediatric-focused information of molecular targets to guide decisions around pediatric development of a given drug asset (143). Drugs targeting molecules contained within the Pediatric Molecular Targets List may prompt industry collaborators to engage preclinical testing groups, which initiates the process of establishing collaborative work agreements, preclinical testing plan development, material transfer, PDX model establishment, and testing and analysis of testing data, a process which is typically achieved within a year depending on the complexity of the preclinical study (144). Efforts within the COG Bone Tumor Committee and PIVOT are underway to coordinate the development, prioritization, and testing of drugs and drug targets with the goal of facilitating the identification and clinical development of the most promising drugs for Ewing sarcoma. Additionally, a collaborative effort including the NIH, FDA, industry, and knowledge leaders in pediatric oncology convened the Federation for the National Institutes of Health Convening experts in Oncology to Address Children's Health in quarterly meetings from 2022 to 2024 to comprehensively review existing preclinical and clinical data on targets relevant to pediatric oncology with the goal of identifying targets that would benefit from additional preclinical testing and provide consensus recommendations on target prioritizations for pediatric cancer (https://fnih.org/our-programs/convening-experts-in-oncology-to-address-childrens-health-coach/).

Patient Advocacy in Ewing Sarcoma Research

As an additional component to this international collaborative effort, we engaged patient advocates as collaborative partners to help guide preclinical research priorities in Ewing sarcoma. There remains an urgent need to better understand and model disease relapse and resistance. An impediment to improving our understanding of disease relapse and resistance in Ewing sarcoma results, in part, from the infrequent practice for pediatric patients of tissue sampling at times of treatment relapse and disease progression resulting in fewer opportunities for obtaining tissue and generating research models. However, informal surveys of patients and family members around the topic of research-only tumor biopsies or rapid autopsy programs have revealed general favor for participation in these efforts if tissue collection may have the potential to guide care or improve understanding of disease. Partnerships with patient advocates to identify and support programs enabling tumor tissue donation (particularly from relapsed and/or refractory cases via research-only biopsies or rapid autopsy tissue procurement) will be invaluable. These efforts will help expand access to tissue and models that will improve our understanding of disease relapse and resistance, leading to insights into novel therapies for EwS and other cancers.

Conclusions

Although the past decade has yielded significant insights into the genetic landscape of Ewing sarcoma, improved understanding of the role of the EWS::FLI1 fusion in driving Ewing sarcoma biology and multiple agents tested preclinically and clinically for patients with Ewing sarcoma, we continue to struggle in identifying agents that are durably effective in Ewing sarcoma, particularly for patients with relapsed or metastatic disease. Motivated by a collective frustration in the lack of improvement in the survival of patients with high-risk Ewing sarcoma, an increase in the number of potential drugs in the therapeutic armamentarium, and improvements in Ewing sarcoma modeling, we assembled an international collective of investigators to organize a comprehensive catalogue of existing Ewing sarcoma preclinical models, identify gaps in prior preclinical study strategies, and highlight how existing resources can be leveraged to facilitate the identification and clinical translation of active drugs into the clinic for patients with Ewing sarcoma.

A summary of molecular and clinical annotation of Ewing sarcoma preclinical models provided in this review can serve to standardize model referencing in experiments and aid in the rational selection of Ewing sarcoma tumors with specific biological features represented (e.g., STAG2 loss, *TP53* mutant, and *CDKN2A* deleted) to explore differential sensitivities of and resistance to drugs across genomically distinct Ewing sarcoma. We have provided perspectives on the consideration of different *in vivo* model types for use in preclinical studies detailing both immunocompetent and immunodeficient Ewing sarcoma models, the pros and cons of these models, and the effects of different modes of tumor establishment on Ewing sarcoma biology and potential impact on drug responses. Additionally, agents anticipated to elicit immunomodulatory responses

should be considered for testing in models with the appropriate immune cells present. This "right model for the right drug" approach will help continue to develop our understanding of the TME and its impact on Ewing sarcoma cell behavior.

Improved understanding of therapy resistance mechanisms and characterization of resistant Ewing sarcoma subpopulations within individual patients remains a significant challenge. Although the existence of treatment-naïve Ewing sarcoma models is relatively rare, assembly of pre-therapy, as well as longitudinal models (tumor models generated from the same patient using tumors obtained at various timepoints along the therapy continuum) will serve as incredibly valuable tools that can provide insights into primary resistance mechanisms. Hence, studies involving sequential, longitudinal treatment of models mimicking current standard therapies for Ewing sarcoma, genomic characterization of longitudinally treated models, and studies probing drug resistance using available preclinical models should be prioritized. Similarly, efforts to assemble well-annotated paired, longitudinal samples from patients with Ewing sarcoma, and deposition of genomic data in accessible informatics platforms will be equally invaluable in improving our understanding of therapy resistance over time and across Ewing sarcoma subtypes. Incorporation of tumor and blood sample collections before and after therapeutic interventions as correlative biology objectives in future clinical trials in Ewing sarcoma represents opportunities to collect samples and generate models that will be essential in understanding and validating mechanisms of therapy resistance. As an international community, we propose concerted efforts to use existing models (and generation of new ones) in studies focused on understanding tumor subpopulations, tumor evolution, and resistance mechanisms with the spirit of open sharing of data.

We hope the current review serves as a robust preclinical resource for Ewing sarcoma biologists and establishes a roadmap for continued advancement of Ewing sarcoma translational biology from the international community. Our overarching goal is to move the needle toward improving the translation of preclinical findings into successful clinical trials by improving representation of Ewing sarcoma tumor subtypes in vulnerability testing, aligning selected *in vivo* models with the tested drug's proposed mechanism of action, and enhancing our understanding of resistant tumor subpopulations through longitudinal reassessment.

Authors' Disclosures

A. Soragni reports grants from NCI during the conduct of the study, as well as a patent for WO/2022/125585 pending and a patent for WO/2022/125580 pending. A. Shlien reports other support from NewCode Oncology outside the submitted work, as well as a patent for An RNA-Based Tumor Classifier pending to NewCode Oncology. E.R. Lawlor reports grants from NCI, Cure Childhood Cancer Foundation, and Sam Day Foundation outside the submitted work. D.R. Reed reports personal fees from Springworks, Eisai, and Recordati outside the submitted work. P.J. Grohar reports other support from OrphAI therapeutics outside the submitted work. K.M. Bailey reports other support from Merck outside the submitted work. No disclosures were reported by the other authors.

Disclaimer

The content is solely the responsibility of the authors and does not necessarily represent the official views of the NIH.

Acknowledgments

This work was supported in part through the NIH/NCI Cancer Center Support Grant P30 CA008748 and the NCTN Operations Center Grant (U10CA180886). We gratefully acknowledge Lorna Day (Sam Day Foundation), Riva Ariella Ritvo-Slifka (Alan B. Slifka Foundation), and Chris Copland (Sarcoma UK) for their invaluable contributions as patient advocates, whose perspectives enriched the patient advocacy section and highlight the vital role of advocacy in shaping pediatric cancer research priorities.

Note

Supplementary data for this article are available at Molecular Cancer Therapeutics Online (http://mct.aacrjournals.org/).

Received April 29, 2025; revised July 28, 2025; accepted August 29, 2025; posted first September 4, 2025.

References

1. Shulman DS, Whittle SB, Surdez D, Bailey KM, de Álava E, Yustein JT, et al. An international working group consensus report for the prioritization of molecular biomarkers for Ewing sarcoma. NPJ Precis Oncol 2022;6:65.
2. Minas TZ, Surdez D, Javaheri T, Tanaka M, Howarth M, Kang H-J, et al. Combined experience of six independent laboratories attempting to create an Ewing sarcoma mouse model. Oncotarget 2017;8:34141–63.
3. Nanni P, Landuzzi L, Manara MC, Righi A, Nicoletti G, Cristalli C, et al. Bone sarcoma patient-derived xenografts are faithful and stable preclinical models for molecular and therapeutic investigations. Sci Rep 2019;9:12174.
4. Marques Da Costa ME, Zaidi S, Scoazec J-Y, Droit R, Lim WC, Marchais A, et al. A biobank of pediatric patient-derived-xenograft models in cancer precision medicine trial MAPPYACTS for relapsed and refractory tumors. Commun Biol 2023;6:949.
5. Han JJ. FDA Modernization Act 2.0 allows for alternatives to animal testing. Artif Organs 2023;47:449–50.
6. Sertkaya A, Beleche T, Jessup A, Sommers BD. Costs of drug development and research and development intensity in the US, 2000–2018. JAMA Netw Open 2024;7:e2415445.
7. Delattre O, Zucman J, Plougastel B, Desmaze C, Melot T, Peter M, et al. Gene fusion with an ETS DNA-binding domain caused by chromosome translocation in human tumours. Nature 1992;359:162–5.
8. Brohl AS, Solomon DA, Chang W, Wang J, Song Y, Sindiri S, et al. The genomic landscape of the Ewing Sarcoma family of tumors reveals recurrent STAG2 mutation. PLoS Genet 2014;10:e1004475.
9. Orth MF, Surdez D, Faehling T, Ehlers AC, Marchetto A, Grossetête S, et al. Systematic multi-omics cell line profiling uncovers principles of Ewing sarcoma fusion oncogene-mediated gene regulation. Cell Rep 2022;41:111761.
10. Franzetti G-A, Laud-Duval K, van der Ent W, Brisac A, Irondelle M, Aubert S, et al. Cell-to-cell heterogeneity of EWSR1-FLI1 activity determines proliferation/migration choices in Ewing sarcoma cells. Oncogene 2017;36:3505–14.
11. Seong BKA, Dharia NV, Lin S, Donovan KA, Chong S, Robichaud A, et al. TRIM8 modulates the EWS/FLI oncoprotein to promote survival in Ewing sarcoma. Cancer Cell 2021;39:1262–78.e7.
12. Kovar H, Amatruda J, Brunet E, Burdach S, Cidre-Aranaz F, de Alava E, et al. The second European interdisciplinary Ewing sarcoma research summit–a joint effort to deconstructing the multiple layers of a complex disease. Oncotarget 2016;7:8613–24.
13. Flores G, Grohar PJ. One oncogene, several vulnerabilities: EWS/FLI targeted therapies for Ewing sarcoma. J Bone Oncol 2021;31:100404.
14. Kasan M, Geyer FH, Siebenlist J, Sill M, Öllinger R, Faehling T, et al. Genomic and phenotypic stability of fusion-driven pediatric sarcoma cell lines. Nat Commun 2025;16:380.
15. Lamhamedi-Cherradi S-E, Santoro M, Ramammoorthy V, Menegaz BA, Bartholomeusz G, Iles LR, et al. 3D tissue-engineered model of Ewing's sarcoma. Adv Drug Deliv Rev 2014;79:155–71.
16. Ceranski AK, Carreño-Gonzalez MJ, Ehlers AC, Hanssen KM, Gmelin N, Geyer FH, et al. Refined culture conditions with increased physiological relevance uncover oncogene-dependent metabolic signatures in Ewing sarcoma spheroids. Cell Rep Methods 2025;5:100966.

17. Lawlor ER, Scheel C, Irving J, Sorensen PHB. Anchorage-independent multicellular spheroids as an in vitro model of growth signaling in Ewing tumors. Oncogene 2002;21:307–18.
18. Hotfilder M, Sondermann P, Senss A, Van Valen F, Jürgens H, Vormoor J. PI3K/AKT is involved in mediating survival signals that rescue Ewing tumour cells from fibroblast growth factor 2-induced cell death. Br J Cancer 2005;92:705–10.
19. Roundhill EA, Vasconcelos EJ, Westhead DR, Grissenberger S, Distel M, Burchill SA. Abstract 4683: developing human Ewing sarcoma in vitro models to prioritise new treatments. Cancer Res 2023;83(Suppl 7):4683.
20. Hawkins AG, Basrur V, da Veiga Leprevost F, Pedersen E, Sperring C, Nesvizhskii AI, et al. The Ewing sarcoma secretome and its response to activation of Wnt/beta-catenin signaling. Mol Cell Proteomics 2018;17:901–12.
21. Roundhill EA, Chicon-Bosch M, Jeys L, Parry M, Rankin KS, Droop A, et al. RNA sequencing and functional studies of patient-derived cells reveal that neurexin-1 and regulators of this pathway are associated with poor outcomes in Ewing sarcoma. Cell Oncol 2021;44:1065–85.
22. Ye H, Hu X, Wen Y, Tu C, Hornicek F, Duan Z, et al. Exosomes in the tumor microenvironment of sarcoma: from biological functions to clinical applications. J Nanobiotechnol 2022;20:403.
23. Visser LL, Bleijs M, Margaritis T, van de Wetering M, Holstege FCP, Clevers H. Ewing sarcoma single-cell transcriptome analysis reveals functionally impaired antigen-presenting cells. Cancer Res Commun 2023;3:2158–69.
24. Jurj A, Ionescu C, Berindan-Neagoe I, Braicu C. The extracellular matrix alteration, implication in modulation of drug resistance mechanism: friends or foes? J Exp Clin Cancer Res 2022;41:276.
25. Munoz-Garcia J, Jubelin C, Loussouarn A, Goumard M, Griscom L, Renodon-Cornière A, et al. In vitro three-dimensional cell cultures for bone sarcomas. J Bone Oncol 2021;30:100379.
26. Zhao Z, Chen X, Dowbaj AM, Sljukic A, Bratlie K, Lin L, et al. Organoids. Nat Rev Methods Primers 2022;2:94.
27. Drost J, Clevers H. Organoids in cancer research. Nat Rev Cancer 2018;18:407–18.
28. Tuveson D, Clevers H. Cancer modeling meets human organoid technology. Science 2019;364:952–5.
29. Thorel L, Perréard M, Florent R, Divoux J, Coffy S, Vincent A, et al. Patient-derived tumor organoids: a new avenue for preclinical research and precision medicine in oncology. Exp Mol Med 2024;56:1531–51.
30. Bose S, Clevers H, Shen X. Promises and challenges of organoid-guided precision medicine. Med 2021;2:1011–26.
31. Pasch CA, Favreau PF, Yueh AE, Babiarz CP, Gillette AA, Sharick JT, et al. Patient-derived cancer organoid cultures to predict sensitivity to chemotherapy and radiation. Clin Cancer Res 2019;25:5376–87.
32. Friedman AA, Letai A, Fisher DE, Flaherty KT. Precision medicine for cancer with next-generation functional diagnostics. Nat Rev Cancer 2015;15:747–56.
33. Lo Y-H, Karlsson K, Kuo CJ. Applications of organoids for cancer biology and precision medicine. Nat Cancer 2020;1:761–73.
34. Al Shihabi A, Tebon PJ, Nguyen HTL, Chantharasamee J, Sartini S, Davarifar A, et al. The landscape of drug sensitivity and resistance in sarcoma. Cell Stem Cell 2024;31:1524–42.e4.
35. Strauss SJ, Berlanga P, McCabe MG. Emerging therapies in Ewing sarcoma. Curr Opin Oncol 2024;36:297–304.
36. Al Shihabi A, Davarifar A, Nguyen HTL, Tavanaie N, Nelson SD, Yanagawa J, et al. Personalized chordoma organoids for drug discovery studies. Sci Adv 2022;8:eabl3674.
37. Pedace L, Pizzi S, Abballe L, Vinci M, Antonacci C, Patrizi S, et al. Evaluating cell culture reliability in pediatric brain tumor primary cells through DNA methylation profiling. NPJ Precision Oncol 2024;8:92.
38. Ben-David U, Siranosian B, Ha G, Tang H, Oren Y, Hinohara K, et al. Genetic and transcriptional evolution alters cancer cell line drug response. Nature 2018;560:325–30.
39. Polak R, Zhang ET, Kuo CJ. Cancer organoids 2.0: modelling the complexity of the tumour immune microenvironment. Nat Rev Cancer 2024;24:523–39.
40. Scognamiglio G, De Chiara A, Parafioriti A, Armiraglio E, Fazioli F, Gallo M, et al. Patient-derived organoids as a potential model to predict response to PD-1/PD-L1 checkpoint inhibitors. Br J Cancer 2019;121:979–82.
41. Dekkers JF, Alieva M, Cleven A, Keramati F, Wezenaar AKL, van Vliet EJ, et al. Uncovering the mode of action of engineered T cells in patient cancer organoids. Nat Biotechnol 2023;41:60–9.
42. Smith RC, Tabar V. Constructing and deconstructing cancers using human pluripotent stem cells and organoids. Cell Stem Cell 2019;24:12–24.
43. Gordon DJ, Motwani M, Pellman D. Modeling the initiation of Ewing sarcoma tumorigenesis in differentiating human embryonic stem cells. Oncogene 2016;35:3092–102.
44. Marin Navarro A, Susanto E, Falk A, Wilhelm M. Modeling cancer using patient-derived induced pluripotent stem cells to understand development of childhood malignancies. Cell Death Discov 2018;4:7.
45. Rowe RG, Daley GQ. Induced pluripotent stem cells in disease modelling and drug discovery. Nat Rev Genet 2019;20:377–88.
46. Lancaster MA, Knoblich JA. Organogenesis in a dish: modeling development and disease using organoid technologies. Science 2014;345:1247125.
47. Kim J, Koo B-K, Knoblich JA. Human organoids: model systems for human biology and medicine. Nat Rev Mol Cell Biol 2020;21:571–84.
48. Bock C, Datlinger P, Chardon F, Coelho MA, Dong MB, Lawson KA, et al. High-content CRISPR screening. Nat Rev Methods Primers 2022;2:9.
49. Puisieux A, Pommier RM, Morel A-P, Lavial F. Cellular pliancy and the multistep process of tumorigenesis. Cancer Cell 2018;33:164–72.
50. Chen X, Pappo A, Dyer MA. Pediatric solid tumor genomics and developmental pliancy. Oncogene 2015;34:5207–15.
51. Grünewald TGP, Cidre-Aranaz F, Surdez D, Tomazou EM, de Álava E, Kovar H, et al. Ewing sarcoma. Nat Rev Dis Primers 2018;4:5.
52. Sheffield NC, Pierron G, Klughammer J, Datlinger P, Schönegger A, Schuster M, et al. DNA methylation heterogeneity defines a disease spectrum in Ewing sarcoma. Nat Med 2017;23:386–95.
53. Tomazou EM, Sheffield NC, Schmidl C, Schuster M, Schönegger A, Datlinger P, et al. Epigenome mapping reveals distinct modes of gene regulation and widespread enhancer reprogramming by the oncogenic fusion protein EWS-FLI1. Cell Rep 2015;10:1082–95.
54. Boulay G, Sandoval GJ, Riggi N, Iyer S, Buisson R, Naigles B, et al. Cancer-specific retargeting of BAF complexes by a prion-like domain. Cell 2017;171:163–78.e19.
55. Riggi N, Knoechel B, Gillespie SM, Rheinbay E, Boulay G, Suvà ML, et al. EWS-FLI1 utilizes divergent chromatin remodeling mechanisms to directly activate or repress enhancer elements in Ewing sarcoma. Cancer Cell 2014;26:668–81.
56. Moore JB 4th, Loeb DM, Hong KU, Sorensen PH, Triche TJ, Lee DW, et al. Epigenetic reprogramming and re-differentiation of a Ewing sarcoma cell line. Front Cell Dev Biol 2015;3:15.
57. Riggi N, Suvà M-L, Suvà D, Cironi L, Provero P, Tercier S, et al. EWS-FLI-1 expression triggers a Ewing's sarcoma initiation program in primary human mesenchymal stem cells. Cancer Res 2008;68:2176–85.
58. Riggi N, Suvà M-L, De Vito C, Provero P, Stehle J-C, Baumer K, et al. EWS-FLI-1 modulates miRNA145 and SOX2 expression to initiate mesenchymal stem cell reprogramming toward Ewing sarcoma cancer stem cells. Genes Dev 2010;24:916–32.
59. Pfaltzgraff ER, Apfelbaum A, Kassa AP, Song JY, Jiang W, Suhan TK, et al. Anatomic origin of osteochondrogenic progenitors impacts sensitivity to EWS-FLI1-induced transformation. Cancers 2019;11:313.
60. Sole A, Grossetête S, Heintzé M, Babin L, Zaïdi S, Revy P, et al. Unraveling Ewing sarcoma tumorigenesis originating from patient-derived mesenchymal stem cells. Cancer Res 2021;81:4994–5006.
61. Ramachandran B, Rajkumar T, Gopisetty G. Challenges in modeling EWS-FLI1-driven transgenic mouse model for Ewing sarcoma. Am J Transl Res 2021;13:12181–94.
62. Leacock SW, Basse AN, Chandler GL, Kirk AM, Rakheja D, Amatruda JF. A zebrafish transgenic model of Ewing's sarcoma reveals conserved mediators of EWS-FLI1 tumorigenesis. Dis Model Mech 2012;5:95–106.
63. Torchia EC, Boyd K, Rehg JE, Qu C, Baker SJ. EWS/FLI-1 induces rapid onset of myeloid/erythroid leukemia in mice. Mol Cell Biol 2007;27:7918–34.
64. Javaheri T, Sax B, Nivarthi H, Tomazou E, Mikula M, Pencik J, et al. Abstract 61: a mouse model for small round cell tumors induced by the Ewing sarcoma oncogene EWS/FLI1. Cancer Res 2014;74(Suppl 19):61.
65. Tanaka M, Yamazaki Y, Kanno Y, Igarashi K, Aisaki K-i, Kanno J, et al. Ewing's sarcoma precursors are highly enriched in embryonic osteochondrogenic progenitors. J Clin Invest 2014;124:3061–74.
66. Noorizadeh R, Sax B, Javaheri T, Radic-Sarikas B, Fock V, SureshV, et al. YAP1 is a key regulator of EWS::FLI1-dependent malignant transformation upon IGF-1-mediated reprogramming of bone mesenchymal stem cells. Cell Rep 2025;44:115381.

67. Meraz IM, Majidi M, Meng F, Shao R, Ha MJ, Neri S, et al. An improved patient-derived xenograft humanized mouse model for evaluation of lung cancer immune responses. Cancer Immunol Res 2019;7:1267–79.
68. Rosato RR, Dávila-González D, Choi DS, Qian W, Chen W, Kozielski AJ, et al. Evaluation of anti-PD-1-based therapy against triple-negative breast cancer patient-derived xenograft tumors engrafted in humanized mouse models. Breast Cancer Res 2018;20:108.
69. Chen Q, Wang J, Liu WN, Zhao Y. Cancer immunotherapies and humanized mouse drug testing platforms. Transl Oncol 2019;12:987–95.
70. Chuprin J, Buettner H, Seedhom MO, Greiner DL, Keck JG, Ishikawa F, et al. Humanized mouse models for immuno-oncology research. Nat Rev Clin Oncol 2023;20:192–206.
71. Walsh NC, Kenney LL, Jangalwe S, Aryee K-E, Greiner DL, Brehm MA, et al. Humanized mouse models of clinical disease. Annu Rev Pathol 2017;12:187–215.
72. Ellis JM, Henson V, Slack R, Ng J, Hartzman RJ, Katovich Hurley C. Frequencies of HLA-A2 alleles in five U.S. population groups. Predominance of A*02011 and identification of HLA-A*0231. Hum Immunol 2000;61:334–40.
73. Schreeb K, Culme-Seymour E, Ridha E, Dumont C, Atkinson G, Hsu B, et al. Study design: human leukocyte antigen class I molecule A*02-chimeric antigen receptor regulatory T cells in renal transplantation. Kidney Int Rep 2022;7:1258–67.
74. Hess NJ, Brown ME, Capitini CM. GVHD pathogenesis, prevention and treatment: lessons from humanized mouse transplant models. Front Immunol 2021;12:723544.
75. Weisdorf D, El Jurdi N, Holtan SG. The best GVHD prophylaxis: or at least progress towards finding it. Best Pract Res Clin Haematol 2023;36:101520.
76. Blaeschke F, Thiel U, Kirschner A, Thiede M, Rubio RA, Schirmer D, et al. Human HLA-A*02:01/CHM1+ allo-restricted T cell receptor transgenic $CD8^+$ T cells specifically inhibit Ewing sarcoma growth in vitro and in vivo. Oncotarget 2016;7:43267–80.
77. Daley JD, Mukherjee E, Ferraro D, Tufino AC, Bailey N, Bhaskar S, et al. TGFβ inhibition during radiotherapy enhances immune cell infiltration and decreases metastases in Ewing sarcoma. Cancer Res Commun 2025;5:1441–57.
78. Luo W, Hoang H, Liao Y, Pan J, Ayello J, Cairo MS. A humanized orthotopic mouse model for preclinical evaluation of immunotherapy in Ewing sarcoma. Front Immunol 2023;14:1277987.
79. Hidalgo M, Amant F, Biankin AV, Budinská E, Byrne AT, Caldas C, et al. Patient-derived xenograft models: an emerging platform for translational cancer research. Cancer Discov 2014;4:998–1013.
80. Aparicio S, Hidalgo M, Kung AL. Examining the utility of patient-derived xenograft mouse models. Nat Rev Cancer 2015;15:311–6.
81. Rokita JL, Rathi KS, Cardenas MF, Upton KA, Jayaseelan J, Cross KL, et al. Genomic profiling of childhood tumor patient-derived xenograft models to enable rational clinical trial design. Cell Rep 2019;29:1675–89.e9.
82. Stewart E, Federico SM, Chen X, Shelat AA, Bradley C, Gordon B, et al. Orthotopic patient-derived xenografts of paediatric solid tumours. Nature 2017;549:96–100.
83. Sayles LC, Breese MR, Koehne AL, Leung SG, Lee AG, Liu H-Y, et al. Genome-informed targeted therapy for osteosarcoma. Cancer Discov 2019;9:46–63.
84. Kool M, Federico A, Surdez D, Gopisetty A, Saberi-Ansari E, Saint-Charles A, et al. INSP-15. ITCC-P4: a sustainable platform of molecularly well-characterized PDX models of pediatric cancers for high throughput in vivo testing. Neuro-Oncology 2022;24(Suppl_1):i189.
85. Kurmasheva RT, Houghton PJ. The use of pediatric patient-derived xenografts for identifying novel agents and combinations. In: Patient-derived mouse models of cancer: Patient-Derived Orthotopic Xenografts (PDOX). Cham: Springer International Publishing; 2017. p. 133–59.
86. Kim HR, Kang HN, Shim HS, Kim EY, Kim J, Kim DJ, et al. Co-clinical trials demonstrate predictive biomarkers for dovitinib, an FGFR inhibitor, in lung squamous cell carcinoma. Ann Oncol 2017;28:1250–9.
87. Yagishita S, Nishikawa T, Yoshida H, Shintani D, Sato S, Miwa M, et al. Co-clinical study of [fam-] trastuzumab deruxtecan (DS8201a) in patient-derived xenograft models of uterine carcinosarcoma and its association with clinical efficacy. Clin Cancer Res 2023;29:2239–49.
88. Stewart EL, Mascaux C, Pham N-A, Sakashita S, Sykes J, Kim L, et al. Clinical utility of patient-derived xenografts to determine biomarkers of prognosis and map resistance pathways in EGFR-mutant lung adenocarcinoma. J Clin Oncol 2015;33:2472–80.
89. Vargas R, Gopal P, Kuzmishin GB, DeBernardo R, Koyfman SA, Jha BK, et al. Case study: patient-derived clear cell adenocarcinoma xenograft model longitudinally predicts treatment response. NPJ Precision Oncol 2018;2:14.
90. Vassal G, Houghton PJ, Pfister SM, Smith MA, Caron HN, Li X-N, et al. International consensus on minimum preclinical testing requirements for the development of innovative therapies for children and adolescents with cancer. Mol Cancer Ther 2021;20:1462–8.
91. Vasileva E, Warren M, Triche TJ, Amatruda JF. Dysregulated heparan sulfate proteoglycan metabolism promotes Ewing sarcoma tumor growth. Elife 2022;11:e69734.
92. Pascoal S, Grissenberger S, Scheuringer E, Fior R, Ferreira MG, Distel M. Using zebrafish larvae as a xenotransplantation model to study Ewing sarcoma. Methods Mol Biol 2021;2226:243–55.
93. Ai X, Ye Z, Xiao C, Zhong J, Lancman JJ, Chen X, et al. Clinically relevant orthotopic xenograft models of patient-derived glioblastoma in zebrafish. Dis Model Mech 2022;15:dmm049109.
94. Sturtzel C, Grissenberger S, Bozatzi P, Scheuringer E, Wenninger-Weinzierl A, Zajec Z, et al. Refined high-content imaging-based phenotypic drug screening in zebrafish xenografts. NPJ Precis Oncol 2023;7:44.
95. Grissenberger S, Sturtzel C, Wenninger-Weinzierl A, Radic-Sarikas B, Scheuringer E, Bierbaumer L, et al. High-content drug screening in zebrafish xenografts reveals high efficacy of dual MCL-1/BCL-X_L inhibition against Ewing sarcoma. Cancer Lett 2023;554:216028.
96. Molnar C, Reina J, Herrero A, Heinen JP, Méndiz V, Bonnal S, et al. Human EWS-FLI protein recapitulates in Drosophila the neomorphic functions that induce Ewing sarcoma tumorigenesis. PNAS nexus 2022;1:pgac222.
97. Mahnoor S, Molnar C, Velázquez D, Reina J, Llamazares S, Heinen JP, et al. Human EWS-FLI protein levels and neomorphic functions show a complex, function-specific dose–response relationship in Drosophila. Open Biol 2024;14:240043.
98. Perova Z, Martinez M, Mandloi T, Gomez FL, Halmagyi C, Follette A, et al. PDCM Finder: an open global research platform for patient-derived cancer models. Nucleic Acids Res 2023;51:D1360–6.
99. Koc S, Lloyd MW, Grover JW, Xiao N, Seepo S, Subramanian SL, et al. PDXNet portal: patient-derived Xenograft model, data, workflow and tool discovery. NAR cancer 2022;4:zcac014.
100. Rogojina A, Klesse LJ, Butler E, Kim J, Zhang H, Xiao X, et al. Comprehensive characterization of patient-derived xenograft models of pediatric leukemia. Iscience 2023;26:108171.
101. McLeod C, Gout AM, Zhou X, Thrasher A, Rahbarinia D, Brady SW, et al. St. Jude Cloud: a pediatric cancer genomic data-sharing ecosystem. Cancer Discov 2021;11:1082–99.
102. Flores-Toro JA, Jagu S, Armstrong GT, Arons DF, Aune GJ, Chanock SJ, et al. The childhood cancer data initiative: using the power of data to learn from and improve outcomes for every child and young adult with pediatric cancer. J Clin Oncol 2023;41:4045–53.
103. Zhang Z, Hernandez K, Savage J, Li S, Miller D, Agrawal S, et al. Uniform genomic data analysis in the NCI Genomic Data Commons. Nat Commun 2021;12:1226.
104. Anderson ND, de Borja R, Young MD, Fuligni F, Rosic A, Roberts ND, et al. Rearrangement bursts generate canonical gene fusions in bone and soft tissue tumors. Science 2018;361:eaam8419.
105. Vaske OM, Bjork I, Salama SR, Beale H, Tayi Shah A, Sanders L, et al. Comparative tumor RNA sequencing analysis for difficult-to-treat pediatric and young adult patients with cancer. JAMA Netw Open 2019;2:e1913968.
106. Comitani F, Nash JO, Cohen-Gogo S, Chang AI, Wen TT, Maheshwari A, et al. Diagnostic classification of childhood cancer using multiscale transcriptomics. Nat Med 2023;29:656–66.
107. Balamuth NJ, Womer RB. Ewing's sarcoma. Lancet Oncol 2010;11:184–92.
108. Riggi N, Suvà ML, Stamenkovic I. Ewing's sarcoma. N Engl J Med 2021;384:154–64.
109. Apfelbaum AA, Wrenn ED, Lawlor ER. The importance of fusion protein activity in Ewing sarcoma and the cell intrinsic and extrinsic factors that regulate it: a review. Front Oncol 2022;12:1044707.
110. Chaturvedi A, Hoffman LM, Welm AL, Lessnick SL, Beckerle MC. The EWS/FLI oncogene drives changes in cellular morphology, adhesion, and migration in Ewing sarcoma. Genes Cancer 2012;3:102–16.
111. Chaturvedi A, Hoffman LM, Jensen CC, Lin Y-C, Grossmann AH, Randall RL, et al. Molecular dissection of the mechanism by which EWS/FLI

expression compromises actin cytoskeletal integrity and cell adhesion in Ewing sarcoma. Mol Biol Cell 2014;25:2695–709.
112. Ehnman M, Chaabane W, Haglund F, Tsagkozis P. The tumor microenvironment of pediatric sarcoma: mesenchymal mechanisms regulating cell migration and metastasis. Curr Oncol Rep 2019;21:90.
113. McGranahan N, Swanton C. Clonal heterogeneity and tumor evolution: past, present, and the future. Cell 2017;168:613–28.
114. Pérez-González A, Bévant K, Blanpain C. Cancer cell plasticity during tumor progression, metastasis and response to therapy. Nat Cancer 2023;4:1063–82.
115. Wrenn ED, Apfelbaum AA, Rudzinski ER, Deng X, Jiang W, Sud S, et al. Cancer-associated fibroblast-like tumor cells remodel the Ewing sarcoma tumor microenvironment. Clin Cancer Res 2023;29:5140–54.
116. Dasgupta A, Kurenbekova L, Patel TD, Rajapakshe K, Ghosal G, Nirala B, et al. Modeling Ewing sarcoma lung metastasis. Curr Protoc 2023;3:e670.
117. Pedersen EA, Menon R, Bailey KM, Thomas DG, Van Noord RA, Tran J, et al. Activation of Wnt/β-catenin in Ewing sarcoma cells antagonizes EWS/ETS function and promotes phenotypic transition to more metastatic cell states. Cancer Res 2016;76:5040–53.
118. Scannell CA, Pedersen EA, Mosher JT, Krook MA, Nicholls LA, Wilky BA, et al. LGR5 is expressed by Ewing sarcoma and potentiates Wnt/β-catenin signaling. Front Oncol 2013;3:81.
119. Hayashi M, Baker A, Goldstein SD, Albert CM, Jackson KW, McCarty G, et al. Inhibition of porcupine prolongs metastasis free survival in a mouse xenograft model of Ewing sarcoma. Oncotarget 2017;8:78265–76.
120. Mendoza A, Hong S-H, Osborne T, Khan MA, Campbell K, Briggs J, et al. Modeling metastasis biology and therapy in real time in the mouse lung. J Clin Invest 2010;120:2979–88.
121. Astell KR, Sieger D. Zebrafish in vivo models of cancer and metastasis. Cold Spring Harb Perspect Med 2020;10:a037077.
122. Houghton PJ, Morton CL, Tucker C, Payne D, Favours E, Cole C, et al. The pediatric preclinical testing program: description of models and early testing results. Pediatr Blood Cancer 2007;49:928–40.
123. Goldstein SD, Hayashi M, Albert CM, Jackson KW, Loeb DM. An orthotopic xenograft model with survival hindlimb amputation allows investigation of the effect of tumor microenvironment on sarcoma metastasis. Clin Exp Metastasis 2015;32:703–15.
124. Crenn V, Biteau K, Amiaud J, Dumars C, Guiho R, Vidal L, et al. Bone microenvironment has an influence on the histological response of osteosarcoma to chemotherapy: retrospective analysis and preclinical modeling. Am J Cancer Res 2017;7:2333–49.
125. Vormoor B, Knizia HK, Batey MA, Almeida GS, Wilson I, Dildey P, et al. Development of a preclinical orthotopic xenograft model of Ewing sarcoma and other human malignant bone disease using advanced in vivo imaging. PLoS One 2014;9:e85128.
126. Maloney C, Edelman MC, Kallis MP, Soffer SZ, Symons M, Steinberg BM. Intratibial injection causes direct pulmonary seeding of osteosarcoma cells and is not a spontaneous model of metastasis: a mouse osteosarcoma model. Clin Orthop Relat Res 2018;476:1514–22.
127. López-Alemany R, Tirado OM. Metastasis assessment in Ewing sarcoma using orthotopic xenografts. Methods Mol Biol 2021;2226:201–13.
128. Van Noord RA, Thomas T, Krook M, Chukkapalli S, Hoenerhoff MJ, Dillman JR, et al. Tissue-directed implantation using ultrasound visualization for development of biologically relevant metastatic tumor xenografts. In Vivo 2017;31:779–91.
129. Pappo AS, Patel SR, Crowley J, Reinke DK, Kuenkele K-P, Chawla SP, et al. R1507, a monoclonal antibody to the insulin-like growth factor 1 receptor, in patients with recurrent or refractory Ewing sarcoma family of tumors: results of a phase II Sarcoma Alliance for Research through Collaboration study. J Clin Oncol 2011;29:4541–7.
130. Brenner JC, Feng FY, Han S, Patel S, Goyal SV, Bou-Maroun LM, et al. PARP-1 inhibition as a targeted strategy to treat Ewing's sarcoma. Cancer Res 2012;72:1608–13.
131. Smith MA, Houghton PJ, Lock RB, Maris JM, Gorlick R, Kurmasheva RT, et al. Lessons learned from 20 years of preclinical testing in pediatric cancers. Pharmacol Ther 2024;264:108742.
132. Murphy B, Yin H, Maris JM, Kolb EA, Gorlick R, Reynolds CP, et al. Evaluation of alternative in vivo drug screening methodology: a single mouse analysis. Cancer Res 2016;76:5798–809.
133. Gao H, Korn JM, Ferretti S, Monahan JE, Wang Y, Singh M, et al. High-throughput screening using patient-derived tumor xenografts to predict clinical trial drug response. Nat Med 2015;21:1318–25.
134. Meric-Bernstam F, Lloyd MW, Koc S, Evrard YA, McShane LM, Lewis MT, et al. Assessment of patient-derived xenograft growth and antitumor activity: the NCI PDXNet consensus recommendations. Mol Cancer Ther 2024;23:924–38.
135. Ortmann J, Rampášek L, Tai E, Mer AS, Shi R, Stewart EL, et al. Assessing therapy response in patient-derived xenografts. Sci Transl Med 2021;13:eabf4969.
136. Evrard YA, Srivastava A, Randjelovic J, Doroshow JH, Dean DA 2nd, Morris JS, et al. Systematic establishment of robustness and standards in patient-derived xenograft experiments and analysis. Cancer Res 2020;80:2286–97.
137. Houghton PJ, Adamson PC, Blaney S, Fine HA, Gorlick R, Haber M, et al. Testing of new agents in childhood cancer preclinical models: meeting summary. Clin Cancer Res 2002;8:3646–57.
138. Barone A, Casey D, McKee AE, Reaman G. Cancer drugs approved for use in children: impact of legislative initiatives and future opportunities. Pediatr Blood Cancer 2019;66:e27809.
139. Zettler ME. The RACE for children act at one year: progress in pediatric development of molecularly targeted oncology drugs. Expert Rev Anticancer Ther 2022;22:317–21.
140. Federico A, Gopisetty A, Surdez D, Iddir Y, Saint-Charles A, Wierzbinska J, et al. Abstract 3571:The ITCC-P4 sustainable platform of fully characterized PDXs supports the preclinical proof-of-concept drug testing of high-risk pediatric tumor models. Cancer Res 2023;83(Suppl 7):3571.
141. Dela Cruz FS, McCarter JG, You D, Bouvier N, Wang X, Guillan KC, et al. Abstract 704: Development of a patient-derived xenograft (PDX) modeling program to enable pediatric precision medicine. Cancer Res 2022;82(Suppl 12):704.
142. Pearson ADJ, Federico S, Gatz SA, Ortiz M, Lesa G, Scobie N, et al. Paediatric Strategy Forum for medicinal product development of DNA damage response pathway inhibitors in children and adolescents with cancer: ACCELERATE in collaboration with the European Medicines Agency with participation of the Food and Drug Administration. Eur J Cancer 2023;190:112950.
143. US Food and Drug Administration. Pediatric molecular target list. US Food and Drug Administration. [cited 2024 Jan 15]. Available from: https://moleculartargets.ccdi.cancer.gov/fda-pmtl.
144. NCI PIVOT program. [cited 2024 Jan 15]. Available from: https://preclinicalpivot.org/.